

https://doi.org/10.1038/s44304-025-00144-w

Unequal impacts of future droughts on global croplands: contributions of climate and land-use changes across different income groups

Check for updates

Xu Wang¹, Ye Xu¹⊠, Wei Li¹ & Yurui Fan²

This study presents a global assessment of future cropland exposure to drought risks under climate change, accounting for both climate variability and land-use changes across income groups. We used SPI and SPEI to assess concurrent 3- and 6-month drought risks during major crop-growing periods, applying a copula-based method to capture joint and transitional drought events. Exposure disparities and dominant drivers were evaluated using high-resolution global cropland projections under SSP245 and SSP585 scenarios. Results show modest increases in SPI-based severe drought concurrence but substantial increases in extreme droughts, particularly under SSP585. SPEI-based projections reveal even greater risks due to temperature-driven evapotranspiration, with some exposure increases exceeding 4000%. Transitional drought risks further intensify vulnerabilities, especially in lower-middle-income countries. Climate change emerges as the dominant driver of exposure increases, while the role of land-use change diminishes. These findings underscore the urgent need for climate mitigation and targeted adaptation to safeguard global food security.

Global population growth, coupled with rising living standards, has intensified the expansion of agricultural land use, driven by the escalating demand for food, biofuels, and other commodities^{1–3}. Between 2003 and 2019, cropland area expanded by 9%, while cropland net primary production surged by 25%, primarily due to agricultural activities in Africa and South America³. Presently, agricultural land occupies over one-third of the global land area, with cropland comprising approximately 33% of the total agricultural area⁴. As demand for agricultural commodities is projected to rise by 35–56% between 2010 and 2050⁵, pressure on global farming systems will intensify, driving further cropland expansion.

However, global warming poses severe threats to agricultural sustainability, particularly through its impact on drought patterns and severity. The increasing frequency, duration, and intensity of droughts present substantial risks to food security. Recent studies highlight that approximately three-quarters of global harvested land, equating to 454 million hectares, experienced drought-induced yield losses between 1983 and 2009, with cumulative losses valued at 166 billion U.S. dollars. In Europe, droughts have reduced cereal yields by 9% on average between 1964 and 2015, with impacts tripling over the past five decades. Moreover, drought-related crises such as the East African drought of 2011, which resulted in

widespread starvation and displacement^{8,9}, emphasize the need for effective drought mitigation strategies.

There have been a great number of studies to address drought risks through various drought indicators such as Precipitation Index (SPI)¹⁰, Standardized Precipitation Evapotranspiration Index (SPEI)¹¹, Palmer Drought Severity Index¹², standardized soil moisture index¹³. These drought indicators have also been applied to characterize future drought risks under climate change. For instance, Chiang et al.¹⁴ used SPI and SPEI to reveal the impacts of anthropogenic on global drought frequency, duration, and intensity. Wu et al.¹⁵ investigated changes in meteorological and hydrological drought conditions, especially their propagation features in 1.5–3.0 °C warmer climates for 8655 watersheds globally.

Furthermore, these drought indicators have also been employed to assess the impacts of drought on crop production. For instance, Mohammed et al. ¹⁶ utilized SPI and SPEI to evaluate the drought impacts on maize and wheat yields across Hungary during 1961–2010, finding that both crops were highly vulnerable to drought conditions. Similarly, Parsons et al. ¹⁷ characterized the regional relationship between drought impacts occurrence in British agriculture and two drought indices (SPI and SPEI), concluding that SPEI for the preceding six months is the best indicator to predict the

¹MOE Key Laboratory of Regional Energy and Environmental Systems Optimization, College of Environmental Science and Engineering, North China Electric Power University, Beijing, China. ²Department of Civil and Environmental Engineering, Brunel University of London, Middlesex, UK. —e-mail: xuye@ncepu.edu.cn

probability of drought impacts on agriculture in the UK. Additionally, SPI and SPEI have also been used to characterize drought impact on crop productions in other regions such as Nepal¹⁸ and Spain¹⁹.

Recent studies have increasingly focused on assessing the impacts of drought on future agricultural sustainability under various climate change scenarios, utilizing climate and cropland projection datasets. Prodhan et al. 20 projected future drought conditions and their impact on simulated crop yields across South Asia using the SPEI drought index derived from CMIP6 outputs. Their findings revealed a non-linear increase in yield loss risk as drought intensity rises. Wang et al.²¹ evaluated global cropland exposure to compound drought-heatwave extreme events under future climate change, using the standardized dry and hot index. They found that climate effects are expected to be the dominant driving factor behind the increased exposure of croplands. Wang et al.²² developed a probabilistic analysis method to quantify the likelihood of yield loss due to drought in Australia's crop belt, utilizing the 3-month SPEI. Their study suggests that droughts will become more frequent and affect larger areas under future warming scenarios. Mondal et al.²³ used 12-month SPEI to measure south Asian cropland exposure to drought and its underlying factors based on projections from 7 CMIP6 models, indicating that climate change effect is the pivotal contributor in exposure changes over South Asia. Schillerberg and Tian²⁴ assess the current and future global compound climate extreme events, as well as population, agriculture, and forestry exposures to these events, in which agriculture area exposure to the simultaneous heatwave and flash drought were analysed under two climate change scenarios (SSP126 and SSP585).

While numerous studies have used SPI and SPEI indices to assess the impacts of drought on cropland exposure and have identified relevant time scales for agricultural sensitivity, a key gap remains in understanding the transitional dynamics of droughts across time scales and severity levels. Drought is a multifaceted phenomenon, and its progression—from short-term to long-term or from moderate to extreme events—can have compounding impacts on agriculture. Most existing studies analyze individual time scales in isolation or focus on specific drought phases, with limited attention to how drought transitions (e.g., from 3-month severe drought to 6-month extreme drought) affect cropland exposure, particularly at the global level. Our study addresses this gap by systematically quantifying global cropland exposure to compound drought transitions across SPI and SPEI indicators, offering a more dynamic and integrative perspective on agricultural drought risk.

Furthermore, future global drought patterns are expected to exhibit significant spatial and temporal variability. Coupled with socioeconomic development disparities, cropland expansion is likely to vary across countries with different income levels. However, current research has not sufficiently analyzed how cropland expansion and the associated drought exposure risks differ across income levels under varying climate change scenarios. Additionally, most studies focus on the direct impacts of drought events on agriculture without considering the compounded effects of concurrent droughts and transitional drought risks, which could exacerbate agricultural vulnerabilities. The interactions between climate change, landuse dynamics, and their combined effects on drought persistence and intensity remain underexplored. Understanding how temperature-driven evapotranspiration amplifies drought risks, especially under high-emission scenarios, is critical for developing effective adaptation and mitigation strategies.

This study aims to build upon existing research by exploring future drought risks and their potential impacts on croplands at a global scale. Specifically, it will analyze 3- and 6-month droughts characterized by SPI and SPEI, based on climate projections from 12 CMIP6 GCMs under the SSP245 and SSP585 scenarios. These time scales are selected because they broadly capture short- to medium-term agricultural droughts that align with the main growing seasons for major crops in many regions. A copula-based approach will be employed to quantify the concurrence risks of 3- and 6-month droughts and assess the transitional risks of 3-month droughts evolving into 6-month droughts, capturing the persistence and intensification of drought conditions. Furthermore,

utilizing high-resolution projected cropland data under various climate change scenarios, the research will quantify the extent of croplands in countries with different income levels that are threatened by concurrent droughts (3- and 6-month), and drought transitions (from 3-month to 6-month droughts). The study will also evaluate the relative contributions of climate change, land-use dynamics, and their interactions to future cropland exposure, identifying key drivers of agricultural vulnerability. By analyzing exposure disparities across income groups, the research will provide critical insights into the unequal impacts of climate change on global agriculture.

Results

Concurrence risks of 3-month and 6-month droughts

This study quantifies changes in the risk of simultaneous 3-month and 6-month severe (SD3nSD6) and extreme drought (ED3nED6) events under different climate change scenarios. The 3-month period corresponds to April–June in the Northern Hemisphere and October–December in the Southern Hemisphere, while the 6-month period spans April–September in the Northern Hemisphere and October–March in the Southern Hemisphere. These timeframes are crucial for agricultural planning and water resource management, as they align with key crop growth stages. Droughts during these periods can lead to substantial yield losses, posing serious challenges to food security and water availability. The concurrence risks of 3-month and 6-month droughts are estimated using the copula method, as defined in Eqs. (1)–(3).

Figure 1 illustrates changes in the concurrence of SPI-based drought risks between historical and future periods under SSP245 and SSP585. Figure 1a-d depict the spatial variations in drought risk changes, while Fig. 1e-j present histograms showing risk changes across six continents. The results indicate that there are no significant differences in the concurrence of 3-month and 6-month droughts (SD3nSD6) between SSP245 and SSP585. As shown in Figs. 1e-j, under both scenarios, the percentage changes in SD3nSD6 are mostly within the range of [-1, 1], with a small portion of Europe and Africa experiencing an increase of more than 1% under SSP585. However, for simultaneous 3-month and 6-month extreme droughts (ED3nED6), there is a visible increase in some regions, particularly in northern South America and western Europe, especially the Iberian Peninsula. Under the SSP585 scenario, the increase in ED3nED6 risk is even more pronounced. Additionally, certain areas of the Amazon, southern Chile, and parts of western Africa also face an elevated risk of ED3nED6. These findings are further confirmed by the histograms in Fig. 1e-j. The histograms under SSP585 exhibit a longer tail compared to those under SSP245, indicating a higher frequency of extreme drought risk increases. In some regions of Europe and South America, the risk of ED3nED6 may increase by up to 10 percentage points compared to the historical period. In summary, while the concurrence of severe droughts (SD3nSD6) remains largely unchanged under SSP245 and SSP585, the risk of simultaneous extreme droughts (ED3nED6) increases significantly in certain regions, with a more pronounced increase under SSP585.

Compared to SPI, SPEI considers not only precipitation but also potential evapotranspiration (PET), thereby capturing the influence of temperature on drought conditions. Figure 2 illustrates the changes in the concurrence of SPEI-based drought risks between historical and future periods under SSP245 and SSP585. For SD3nSD6 risk, there may be a slight increase in the future; however, the changes remain minimal under both SSP245 and SSP585, as shown in Fig. 2a, b. Additionally, as indicated in Fig. 2e-j, in most regions, the increase in SD3nSD6 risk remains within 5 percentage points under both SSP245 and SSP585. In some areas of Africa, Asia, and North America, the risk may even show a slight decrease. However, when it comes to extreme drought risk (ED3nED6), there are significant increases from northwestern China to most of Europe, as well as in northern Africa and the Arabian Peninsula, even under the SSP245 scenario. Under SSP585, both the magnitude of ED3nED6 risk increase and the affected regions expand substantially. As presented in Fig. 2d, higher ED3nED6 risks are observed across a broad

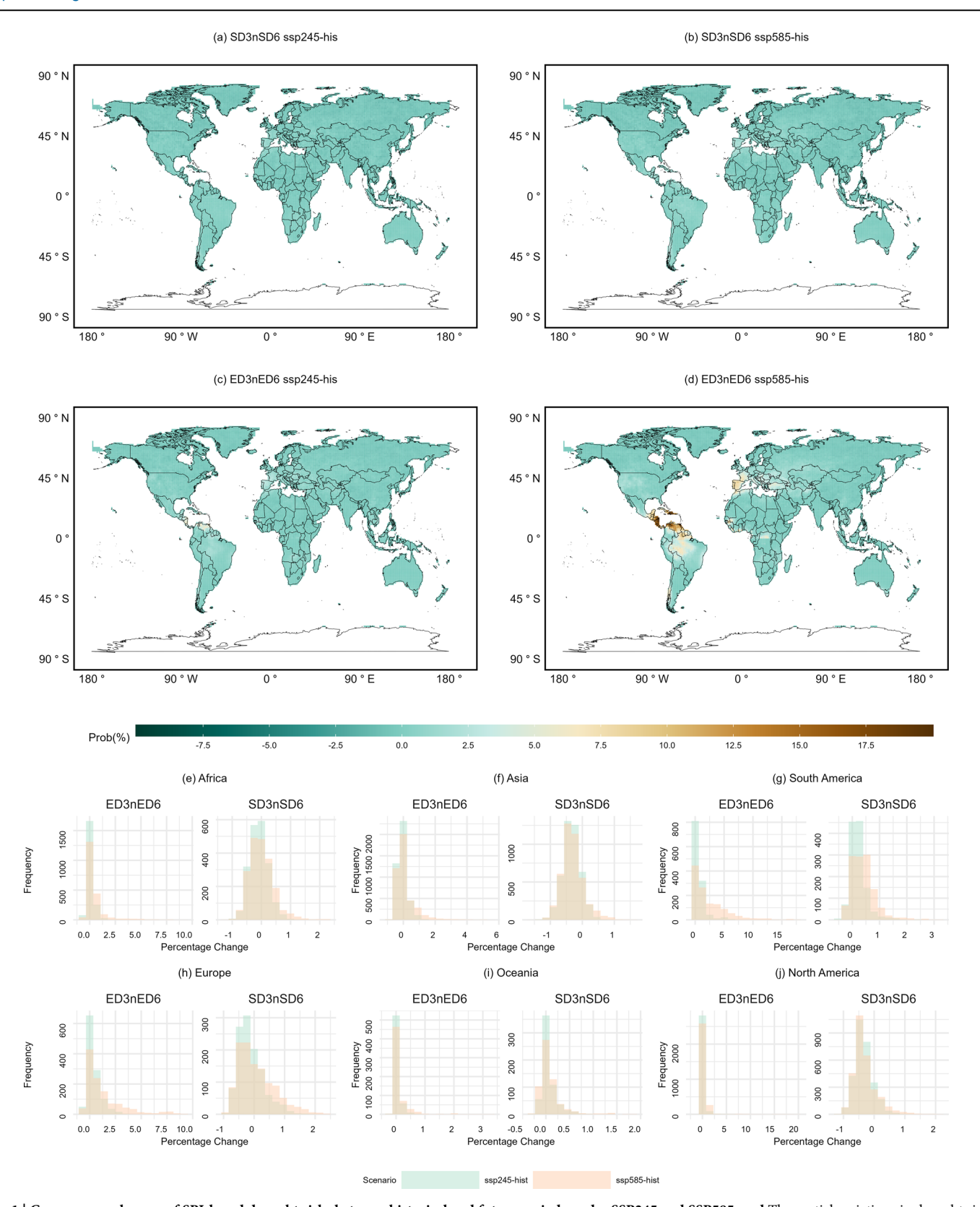


Fig. 1 | Concurrence changes of SPI-based drought risks between historical and future periods under SSP245 and SSP585. a-d The spatial variations in drought risk changes. e-j Histograms showing risk changes across six continents.

area, including northwestern China, most of Europe, northern and southern Africa, the Arabian Peninsula, the U.S. Midwest—particularly southern California—as well as from Central America to much of the Amazon, central to southern Chile, and central and western Australia. As shown in the histograms in Figs. 2e–j, except for some regions in

Africa, most other areas experience an ED3nED6 risk increase of within 20 percentage points compared to the historical period under SSP245. However, under SSP585, the histograms exhibit a much more pronounced right tail than those under SSP245, with many regions in Africa, Asia, and Europe experiencing risk increases of more than 20 percentage

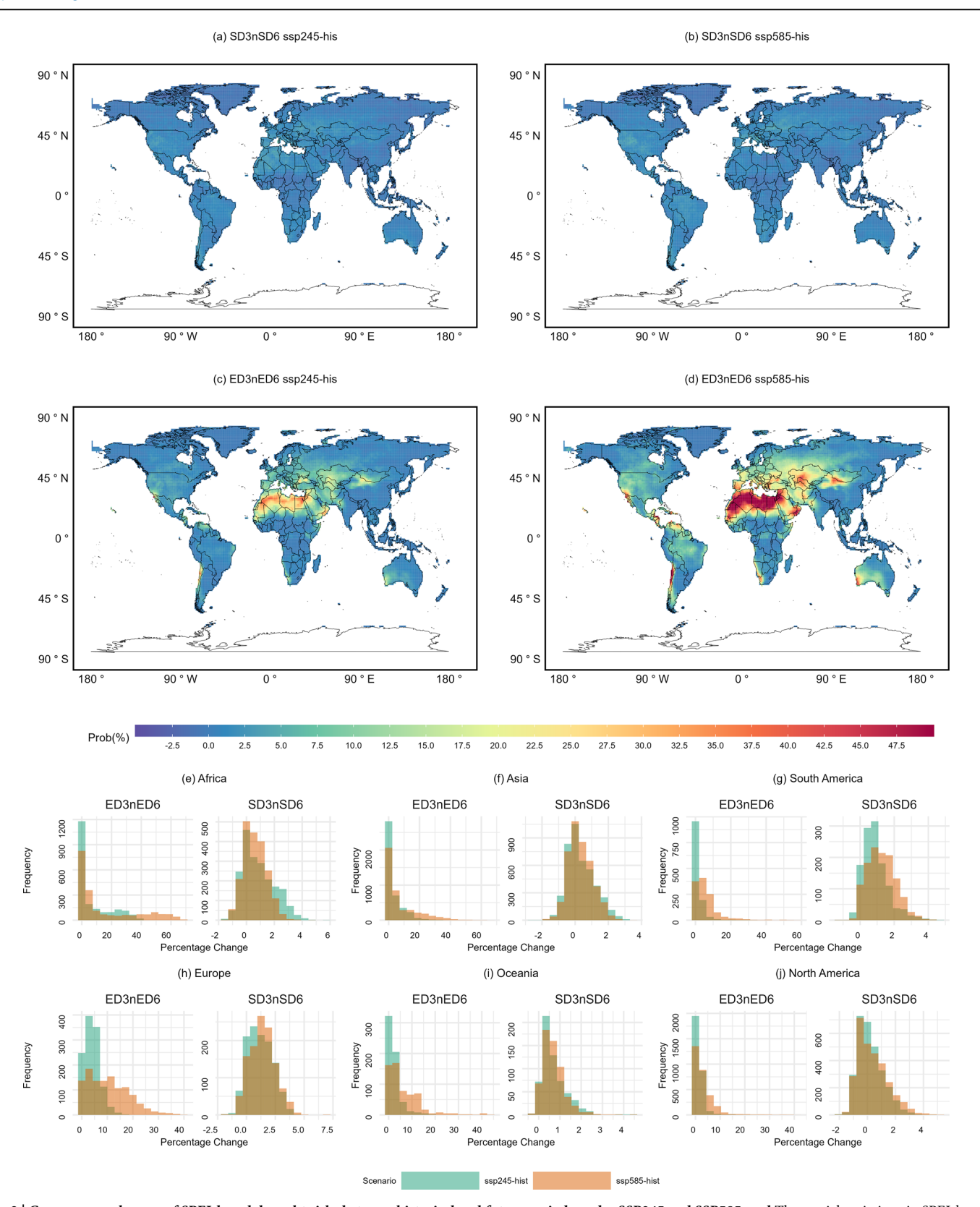


Fig. 2 | Concurrence changes of SPEI-based drought risks between historical and future periods under SSP245 and SSP585. a-d The spatial variations in SPEI-based drought risk changes. e-j Histograms showing SPEI-based risk changes across six continents.

points, and some areas in Africa seeing increases of over 60 percentage points. Overall, while the risk of simultaneous severe droughts (SD3nSD6) under SPEI remains relatively stable with only minor increases, the risk of extreme droughts (ED3nED6) shows significant growth, particularly under SSP585. This increase is especially

pronounced in northwestern China, most of Europe, northern and southern Africa, the Arabian Peninsula, the U.S. Midwest, Central America, the Amazon, central to southern Chile, and western and central Australia, with some regions experiencing risk increases exceeding 60 percentage points.

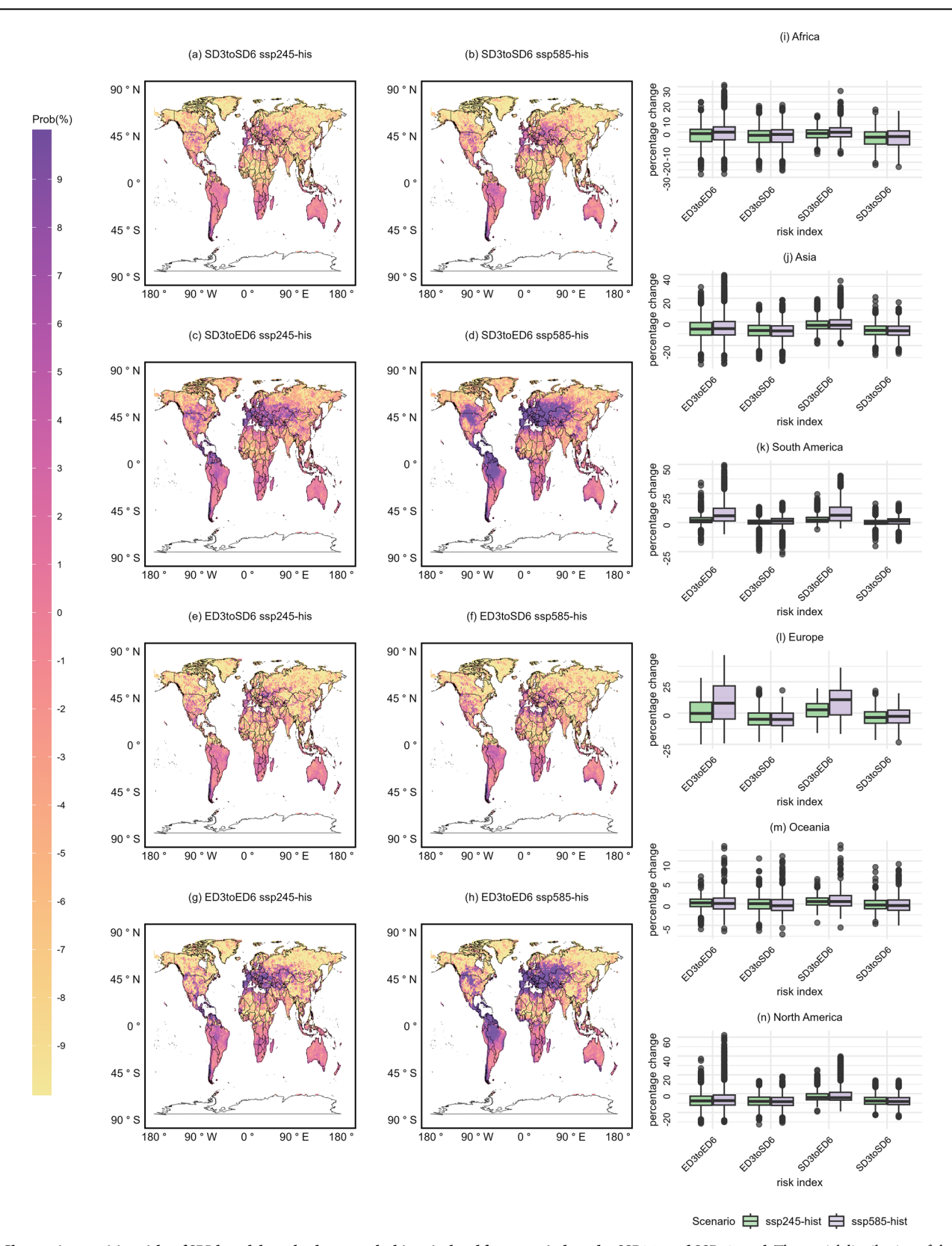


Fig. 3 | Changes in transition risks of SPI-based droughts between the historical and future periods under SSP245 and SSP585. a-h The spatial distribution of changes in SPI-based drought transition risks. i-n Boxplots illustrating the changes in transition risks from 3-month to 6-month SPI-based droughts across the six continents.

Change of drought transition risks

Based on copula-based joint risk analyses for 3-month and 6-month severe and extreme droughts, the transition probabilities were derived using Eq. (4a) to quantify the risks of transitioning from a 3-month severe or extreme drought to a 6-month severe or extreme drought (i.e., SD3toSD6,

SD3toED6, ED3toSD6, and ED3toED6). Figure 3 illustrates the changes in transition risks of SPI-based droughts between historical and future periods under SSP245 and SSP585. Overall, on a global scale, the probability of a 3-month severe or extreme drought transitioning into a 6-month severe drought (i.e., SD3toSD6 and ED3toED6) does not exhibit significant

changes compared to the historical period. Additionally, the impact of different climate change scenarios (SSP245 and SSP585) on these transition probabilities appears to be invisible. This trend is further confirmed by the boxplots on SD3toSD6 and ED3toED6 in Fig. 3i–n, where no substantial differences are observed between SSP245 and SSP585 across all six continents. However, as evident from Fig. 3, a 3-month severe or extreme drought is more likely to transition into an extreme drought in the future, particularly across a vast region extending from Central Asia to most of Europe, as well as in central North America, much of South America, and southern Africa. This increased risk of transitioning to an extreme drought is even more pronounced under the SSP585 scenario especially in Europe and South America. In some regions, the transition risk is expected to rise by more than 20 percentage points under SSP585.

For the transition risk changes in SPEI-based droughts, there are no significant changes in the likelihood of a severe or extreme drought transitioning into an extreme drought in the future, as shown in Fig. 4. Additionally, these minimal changes are not influenced by different climate change scenarios, mirroring the pattern observed in SPI-based drought transitions. Furthermore, as illustrated in the boxplots in Fig. 4i-n, most regions in Africa, Asia, and North America may experience slight decreases in the future probabilities of transitioning from a 3-month severe or extreme drought to a 6-month severe drought (i.e., SD3toSD6, ED3toED6). Nevertheless, a 6-month extreme drought is much more likely to develop from a 3-month severe or extreme drought under future scenarios, with transition probabilities significantly higher than those based on SPI presented in Fig. 3. As shown in Fig. 4c, d, g, h, the probability of a 3-month severe or extreme drought evolving into a 6-month extreme drought increases notably compared to the historical period, particularly in central and western Eurasia, northern Africa, central and western North America, northern South America, and southwestern Australia. This increase is even more severe in both magnitude and spatial extent under SSP585. In particular, central and western Asia, most of Europe, and northern Africa may experience transition risk increases exceeding 50 percentage points. Furthermore, as indicated in the boxplots in Fig. 4i-n, transition risks on SD3toED6 and ED3toED6 have generally increased across most regions on all six continents compared to the historical period, with this increase being even more pronounced under SSP585.

Overall, the transition risk analysis reveals distinct differences between SPI-based and SPEI-based drought projections. While both indices indicate slight changes in the likelihood of a 3-month severe or extreme drought transitioning into a 6-month severe drought (SD3toSD6, ED3toSD6), they both suggest future increases in the probability of a severe or extreme drought developing into an extreme drought (SD3toED6, ED3toED6). However, SPEI-based results indicate a significantly higher probability of transitioning to a 6-month extreme drought. The increased transition risks under SPEI highlight the amplifying effect of temperature-driven evapotranspiration on drought persistence. Under SSP585, these risks become even more pronounced, particularly across central and western Eurasia, northern and southern Africa, North and South America, and southwestern Australia, with some regions experiencing transition risk increases exceeding 50 percentage points. These findings underscore the importance of considering both precipitation and temperature effects when assessing future drought risks.

Crop land exposure to future droughts

The 3-month (April–June in the Northern Hemisphere, October–December in the Southern Hemisphere) and 6-month (April–September in the Northern Hemisphere, October–March in the Southern Hemisphere) drought periods were selected as they encompass the primary growing seasons for major crops. Cropland changes under SSP245 and SSP585 were derived from the 1-km global cropland dataset developed by Cao et al. (2021). The exposure of croplands to droughts was then projected using Eq. (5).

Figure 5 presents the cropland exposure changes to SPI-based 3-month and 6-month severe and extreme drought risks between historical and

future periods. Figure 5a, b show the global distribution of changes in cropland exposure to simultaneous 3-month and 6-month severe droughts (SD3nSD6) under SSP245 and SSP585 relative to the historical period. The increases in cropland exposure to SPI-based SD3nSD6 are relatively moderate across most regions under both SSP245 and SSP585, except for some explicit increases under SSP585 in areas such as Europe, western Africa, and southwestern Australia. However, for ED3nED6, it is apparent that the increase in cropland exposure to (ED3nED6) is much larger than SD3nSD6, highlighting the growing risk of prolonged and intense droughts affecting agriculture. Moreover, cropland exposure risks increase under both scenarios, but SSP585 shows a far more significant escalation, especially across western Asia to most of Europe, Central America, southern Brazil, western Africa, and much of the Indochinese Peninsula.

To further analyze the unequal cropland exposure to droughts, we examine cropland exposure to 3-month and 6-month drought risks across high-income (HI), upper-middle-income (UMI), lower-middle-income (LMI), and low-income (LI) countries, following the World Bank's 2022 classification criteria. As shown in Fig. 5e, under SSP245, the global cropland exposure to SD3nSD6 increases slightly (<2.5%), with the highest rise (~12.5%) in UMI countries, while HI countries see a slight decrease. Under SSP585, exposure increases more visible (~12.5% globally), with HI countries experiencing the highest rise (>15%), followed by UMI and LI countries. Nevertheless, the increase in cropland exposure to ED3nED6 is much more substantial, as shown in Fig. 5f, with future exposure doubling under SSP245 and quadrupling under SSP585 compared to the historical period. Moreover, cropland exposure changes under SSP245 remain relatively stable across the four income groups. However, under SSP585, exposure becomes more unequal, with LMI countries experiencing the highest increase (>350%), while HI countries see the lowest increase (just above 250%).

The cropland exposure changes to SPEI-based drought are presented in Fig. 6. In detail, Fig. 6a, b show the spatial distribution of cropland exposure changes to simultaneous 3-month and 6-month severe droughts (SD3nSD6) under SSP245 and SSP585 compared to the historical period. The increases in cropland exposure are relatively widespread but moderate across most regions, with no significant differences observed between SSP245 and SSP585 in terms of cropland exposure changes. This is further supported by Fig. 6e, which shows that cropland exposure to SD3nSD6 will more than double under both SSP245 and SSP585. However, except for LMI countries, the other three income groups do not exhibit significant differences in the change rate of cropland exposure between the historical and future periods under SSP245 and SSP585. However, the results in Fig. 6c, d show that the increase in exposure to extreme drought concurrence is substantially higher than for severe droughts, particularly under SSP585. The most affected regions include western and central Asia, most of Europe, the North African Mediterranean coast, central North America, and western Africa. Moreover, some hotspot regions, such as western Asia and Europe, experience extreme increases in cropland exposure, with significantly higher exposure under SSP585 than SSP245. Meanwhile, the significant increases in cropland exposure to SPEI-based ED3nED6 also contribute to regional disparities in cropland exposure, as shown in Fig. 6f. Under SSP245, cropland exposure to ED3nED6 increases by 2000% globally, with the highest increase (>2750%) observed in LMI countries and the lowest (~1600%) in HI countries. Under SSP585, the global increase exceeds 4200%, with LMI countries experiencing the highest rise (~5000%), while HI countries see the lowest increase (~3750%). These results indicate that LMI countries face the most severe increases in cropland exposure to extreme drought concurrence, highlighting the unequal impacts of climate change on global agriculture.

Crop land exposure to future drought transition

Due to future climate change, a 3-month severe or extreme drought may evolve into a 6-month severe or extreme drought, as shown in Figs. 3 and 4, posing a significant threat to agricultural sustainability. The changes in cropland exposure to SPI-based drought transition risks between the

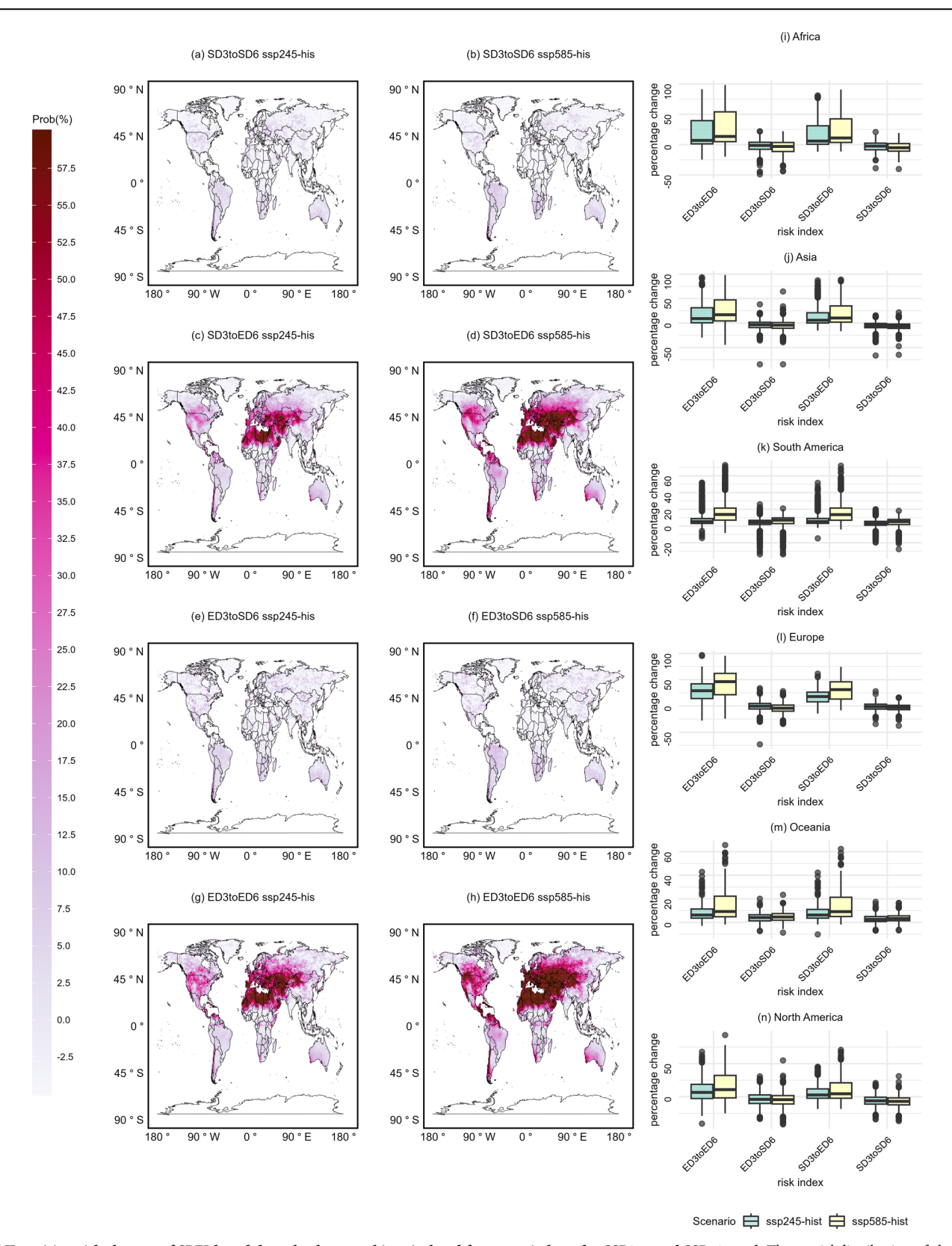


Fig. 4 | Transition risk changes of SPEI-based droughts between historical and future periods under SSP245 and SSP585. a-h The spatial distribution of changes in SPEI-based drought transition risks. i-n Boxplots illustrating the changes in transition risks from 3-month to 6-month SPEI-based droughts across the six continents.

historical and future periods are shown in Fig. 7. It appears that, while there are noticeable increases in cropland exposure to SD3toSD6 in certain regions (e.g., central United States and southwestern Russia to eastern Ukraine), most areas exhibit moderate changes, even under SSP585, as shown in Fig. 7a, b. In fact, the total cropland exposure to SD3toSD6 shows a

declining trend in the future, as illustrated in Fig. 7i, with a decrease of approximately 15% under SSP245 and 20% under SSP585. Moreover, cropland in UMI and LMI countries experiences the highest decline rates, reaching nearly 20% under SSP245 and exceeding 30% under SSP585. A similar pattern is observed for cropland exposure to risks from a 3-month

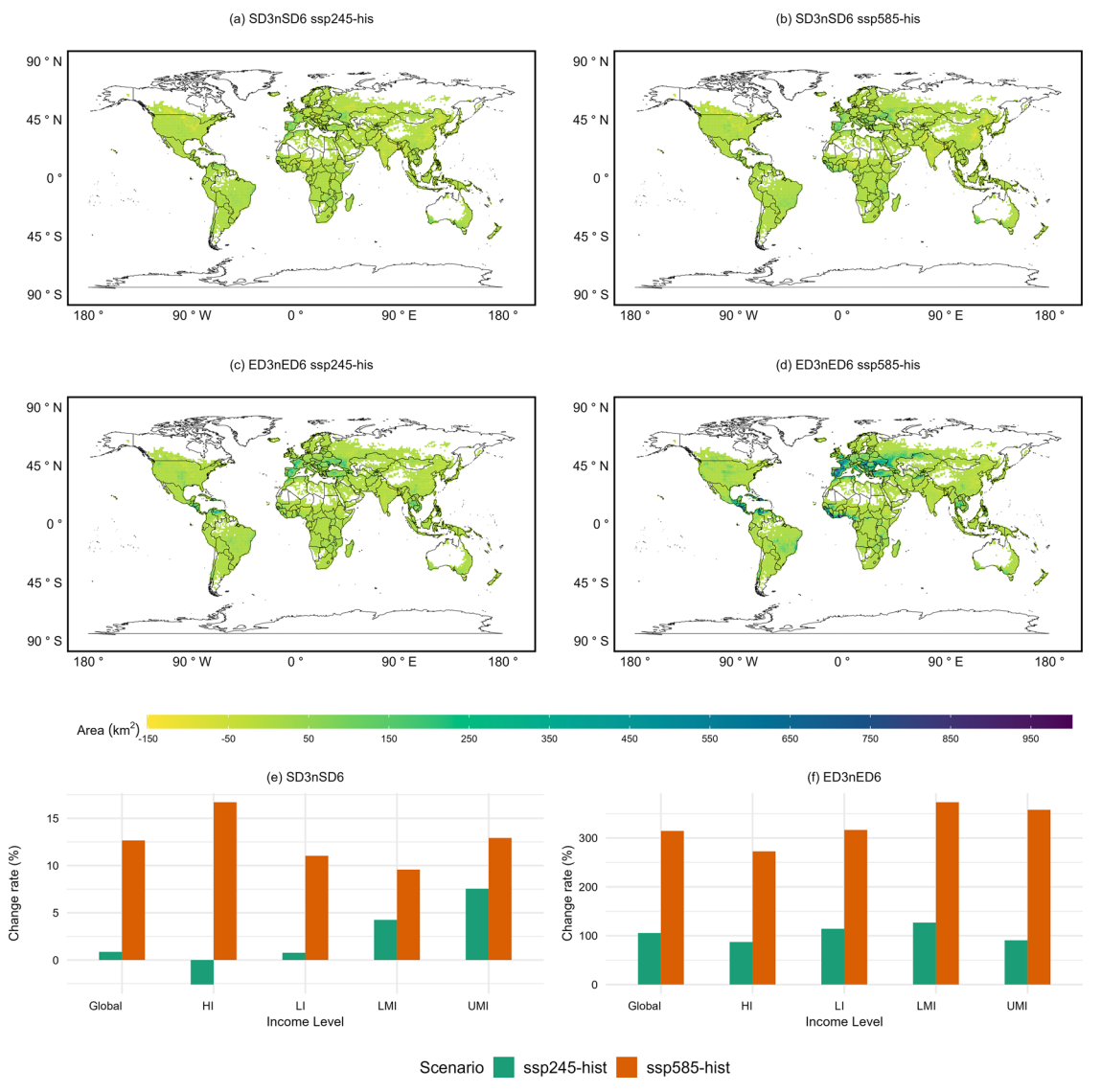


Fig. 5 | Cropland exposure changes to SPI-based drought concurrence risks between historical and future periods under SSP245 and SSP585, a–d The spatial variations in cropland exposure changes to SPI-based droughts. e Bar plot showing global and income-group averaged changes in cropland exposure to simultaneous

3-month and 6-month severe drought. f Bar plot showing global and income-group averaged changes in cropland exposure to simultaneous 3-month and 6-month extreme drought.

extreme drought transitioning to a 6-month severe drought (ED3toSD6), as shown in Fig. 7e, f, k. A declining trend in cropland exposure to ED3toSD6 is expected in future, with a decrease rate exceeding 15% under SSP245 (ranging from 5% for LMI countries to over 20% for HI countries) and greater than 25% under SSP585 (ranging between 25 and 30% across all income groups).

Nevertheless, cropland exposure to 3-month severe or extreme droughts is more likely to transition into 6-month extreme droughts, as shown in Fig. 7c, d, j for SD3toED6, and Fig. 7g, h, l for ED3toED6. Additionally, cropland exposure to SD3toED6 shows explicit increases under future climate change scenarios. Globally, exposure increases moderately under SSP245, with an average rise of around 30%, ranging from ~7% for LMI countries to ~40% for HI countries. However, under SSP585, cropland exposure to SD3toED6 increases substantially, particularly across western Asia to most of Europe, central North America, and Central America, with a global increase rate exceeding 75% and more than doubling for HI countries. The cropland exposure to ED3toED6 follows a similar pattern to SD3toED6, but with a relatively lower increase rate. Globally, exposure rises by less than 10% under SSP245 and then increases to over 35% under SSP585. Notably, UMI countries show a declining trend in

ED3toED6 exposure, likely due to the combined effects of changes in ED3toED6 risks and cropland distribution.

Cropland exposure changes to SPEI-based drought transition risks between historical and future periods are presented in Fig. 8. While cropland exposure to drought transitions into 6-month severe droughts (SD3toSD6, ED3toSD6) decreases under SSP245, similar to SPI-based drought transitions, visible increases are observed under SSP585. Notably, SD3toSD6 exposure rises in HI and LI countries, while ED3toSD6 exposure increases in LI, LMI, and UMI countries. In comparison, cropland exposure to 3-month severe or extreme droughts transitioning into 6-month extreme droughts (SD3toED6 and ED3toED6) will experience substantial increases. While the hotspots for these transitions remain similar to SPI-based results, including central North America, western Asia, most of Europe, and southwestern Australia, the exposure areas under SPEI-based projections are significantly larger than those in SPI-based results, highlighting the greater impact of temperature-driven evapotranspiration on drought persistence and expansion. Income-based disparities are moderate under SSP245, with a global increase rate of 250% for SD3toED6 (Fig. 8j), ranging from ~220% for UMI countries to ~290% for HI countries. For ED3toED6 shown in Fig. 8i, the global average increase is ~240%, with country-level variations ranging

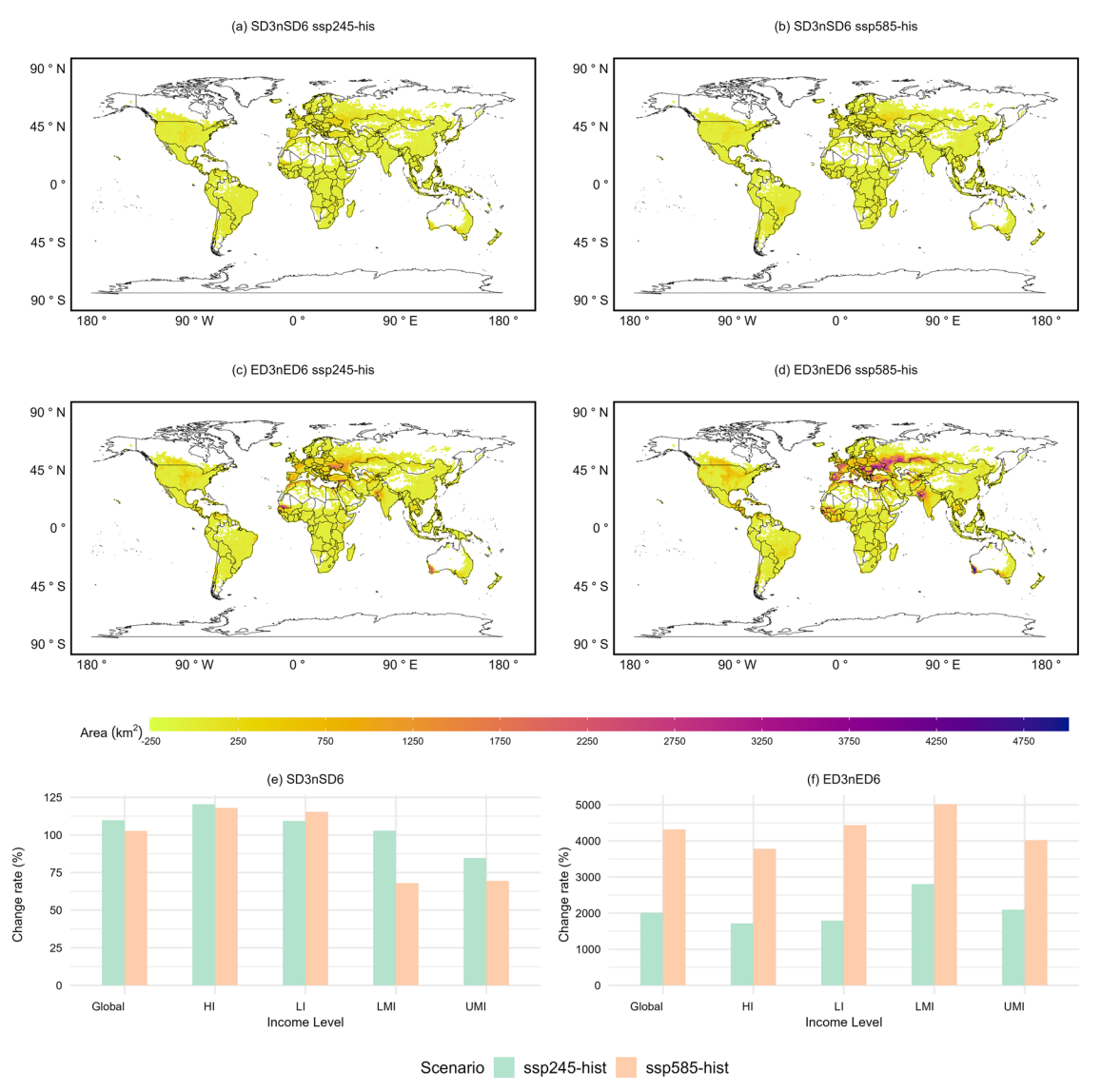


Fig. 6 | Cropland exposure changes to SPEI-based drought concurrence risks between historical and future periods under SSP245 and SSP585. a–d The spatial variations in cropland exposure changes to SPEI-based droughts. e Bar plot showing global and income-group averaged changes in cropland exposure to simultaneous

3-month and 6-month severe drought. f Bar plot showing global and income-group averaged changes in cropland exposure to simultaneous 3-month and 6-month extreme drought.

from 210% for UMI countries to 250% for LMI countries. However, high GHG emissions (SSP585) not only increase cropland exposure but also amplify disparities among income groups. As shown in Fig. 8j, global exposure to SD3toED6 is expected to rise by 350%, with HI countries experiencing the highest increase (450%) and UMI countries the lowest (250%). A similar pattern is observed for ED3toED6, with a global increase of around 320%, ranging from 250% for UMI countries to 350% for HI countries, indicating that higher emissions exacerbate both overall drought risks and income-based inequalities in cropland exposure.

To further investigate the unequal impacts of future drought risks on cropland, the projected changes in cropland exposure to SPI-based and SPEI-based drought risks for the top ten cereal-producing countries were characterized under SSP245 and SSP585 scenarios, as shown in Figs. S2 and S3. Figure S2 shows that projected cropland exposure to SPI-based drought transitions varies substantially across major cereal producers. For moderate-to-moderate drought transitions such as SD3nSD6 and SD3toSD6, increases in exposure are relatively modest and generally below 300%, with stronger changes observed under SSP585. For example, Brazil and Australia exhibit increases of 200–300% in SD3nSD6 exposures under

SSP585, while countries like the USA, China, and India show limited or even negative changes. For more intense transitions, such as ED3nED6, Brazil shows the largest increase, exceeding 1500% under SSP585, followed by Australia and France (~500-800%). These three countries also face substantial risks associated with 3-month droughts transitioning into 6-month extreme droughts (i.e., SD3toED6 and ED3toED6). In contrast, Fig. S3 illustrates substantially higher exposure rates when PET is incorporated into the drought metric via SPEI. Under SSP585, exposure increases for compound droughts (e.g., SD3toED6 or ED3nED6) are exceptionally high. For example, in ED3nED6, Brazil's cropland exposure increases by nearly 20,000%, while France and Russia experience increases above 5000%. These dramatic surges highlight the amplifying effect of PET-especially temperature-driven evapotranspiration—on drought severity under highemission scenarios. Notably, SPEI-based transitions to extreme droughts increase substantially across most countries under SSP585, underscoring the significant impact of greenhouse gas emissions on future agricultural drought risks.

In general, while cropland exposure to drought transitions into 6-month severe droughts shows a declining trend in some regions, the

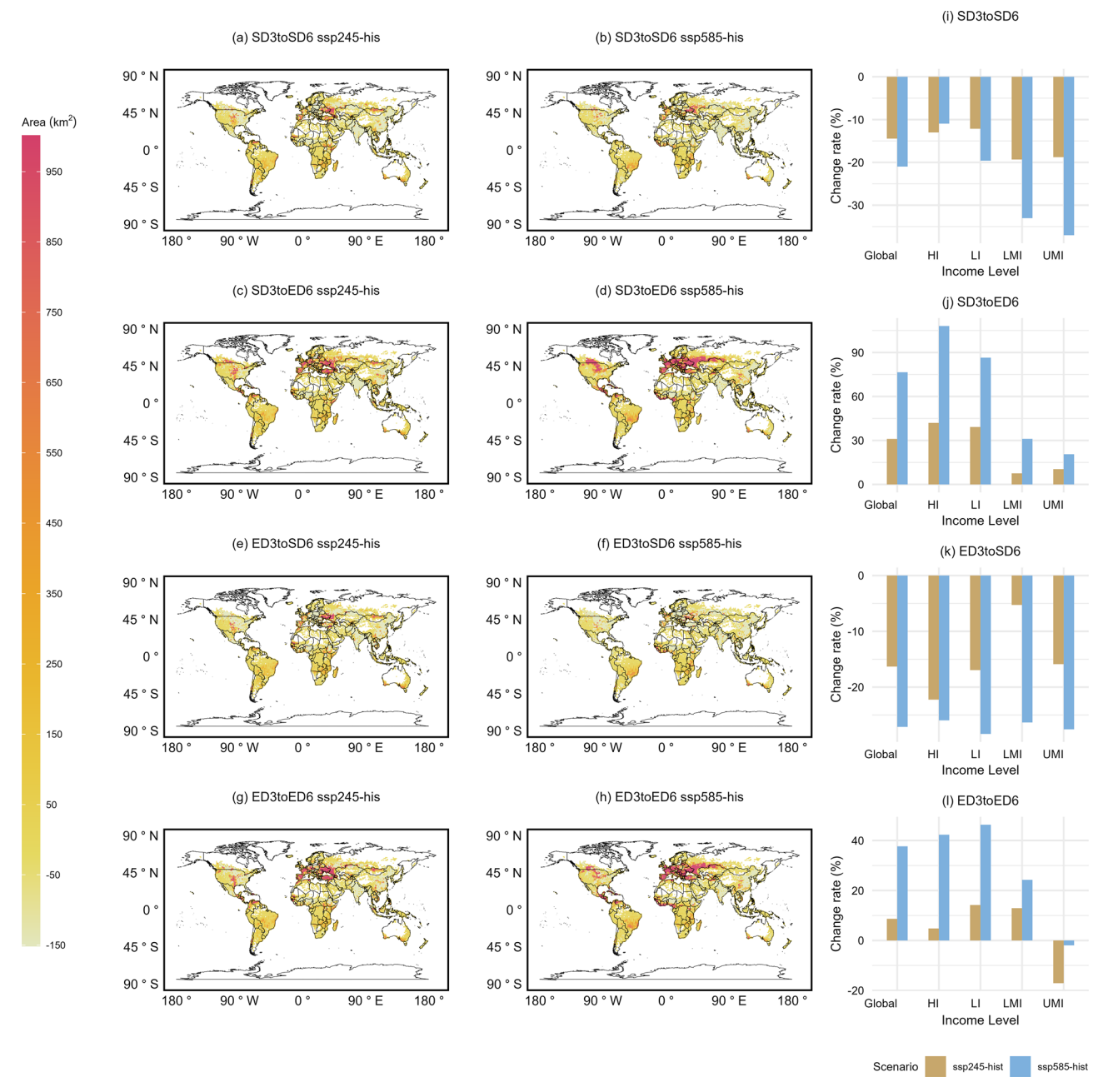


Fig. 7 | Cropland exposure changes to SPI-based drought transition risks between historical and future periods under SSP245 and SSP585. a—h the spatial variations in cropland exposure changes to SPI-based drought transition risks. i—l bar plot

showing global and income-group averaged changes in cropland exposure to different SPI-based drought transition risks.

likelihood of severe or extreme droughts intensifying into prolonged extreme droughts increases substantially, especially under high-emission scenarios. SPEI-based projections indicate larger affected areas compared to SPI-based results, highlighting the amplifying effect of temperature-driven evapotranspiration on drought persistence. Moreover, higher emissions exacerbate disparities in cropland exposure among income groups, with developing regions facing greater vulnerability. These findings emphasize the urgent need for adaptation strategies to mitigate increasing agricultural drought risks under future climate conditions.

Contributions

The cropland exposure to future drought risks is influenced by both climate change and cropland variations, with their relative contributions varying across different climate change scenarios. Based on Eqs. (6) and (4d), the

relative contributions of climate, cropland, and their interaction effects are quantified to identify the dominant factors influencing cropland exposure to different drought events. Specifically, the contributions from climate, cropland, and their interaction effects were calculated for each grid, and the average contributions were determined using a weighted mean based on future cropland exposure at both the global scale and across different income groups.

As shown in Fig. 5, cropland exposure to SPI-based SD3nSD6 exhibits only a minor increase under SSP245, while the increase becomes more pronounced, exceeding 10%, under SSP585. Figure 9a indicates that climate change predominantly drives changes in cropland exposure to SD3nSD6, contributing approximately 67% globally under SSP245, but its influence varies significantly across income groups, revealing clear disparities. Climate change contributes more than 75% to SD3nSD6 exposure in HI and LMI

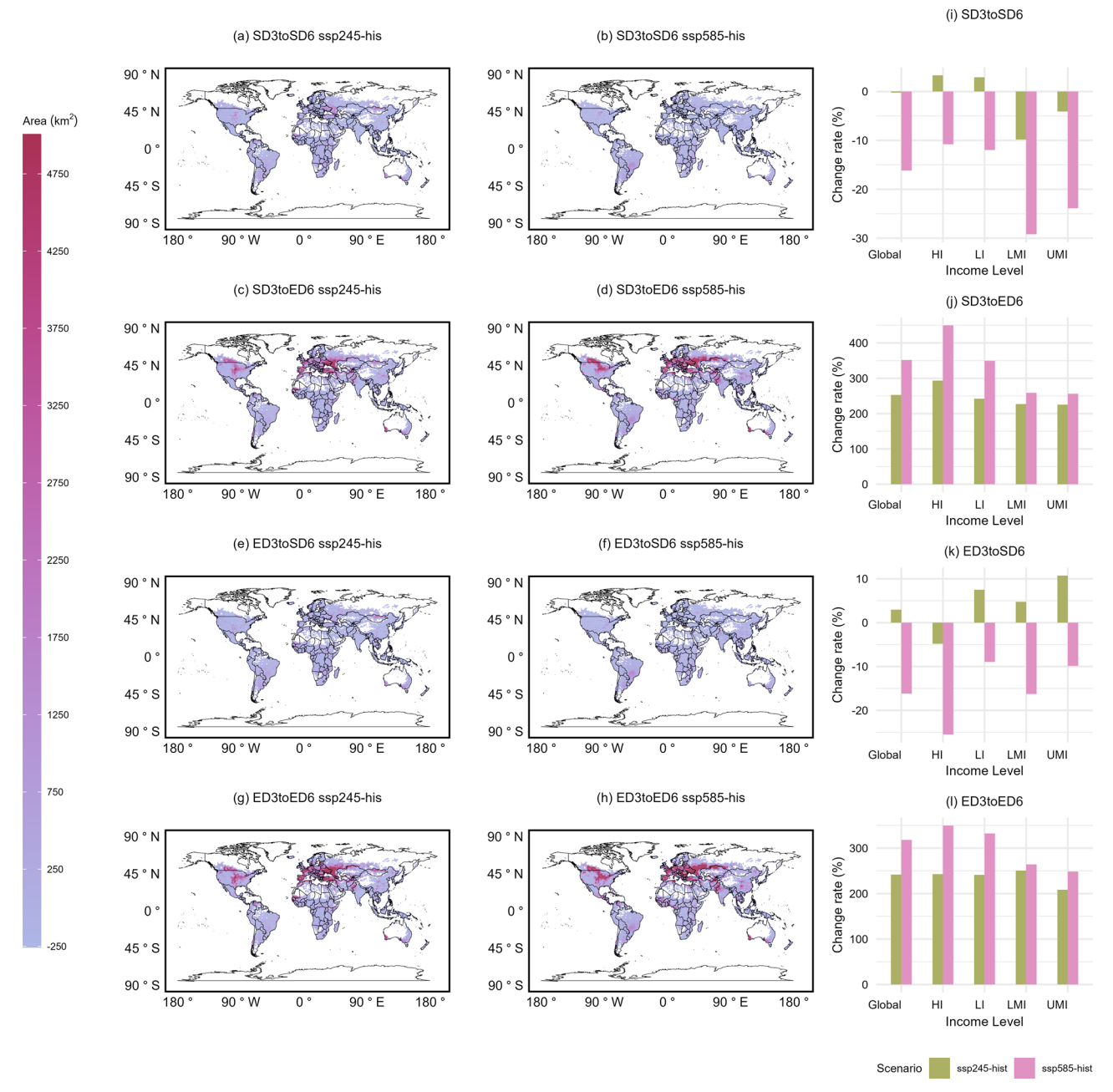


Fig. 8 | Cropland exposure changes to SPEI-based drought transition risks between historical and future periods under SSP245 and SSP585. a—h the spatial variations in cropland exposure changes to SPEI-based drought transition risks.

i-I bar plot showing global and income-group averaged changes in cropland exposure to different SPEI-based drought transition risks.

countries, whereas in UMI and LI countries, cropland variations and interaction effects play a much greater role—with cropland contributing 56% in UMI countries and interaction effects accounting for 39.2% in LI countries, suggesting that lower-income regions experience a more complex interplay of climate and land-use factors. Under SSP585, exposure increases are overwhelmingly driven by climate change (98.5% globally, Fig. 9a), further amplifying inequalities, as cropland variations become negligible in HI and UMI countries but still contribute around 25% in LMI countries and -14.6% in LI countries, indicating that cropland changes in LI countries may even counteract some climate-driven exposure increases.

For SPI-based ED3nED6, cropland exposure is projected to double under SSP245 and quadruple under SSP585 (Fig. 5), further exacerbating inequality in drought risk exposure. The contributions to these increases, presented in Fig. 9b, show that climate change remains the dominant factor,

contributing 109.8% under SSP245 and 98.7% under SSP585 globally. However, the magnitude of climate influence and the role of cropland changes vary among income groups, reinforcing unequal drought vulnerabilities. In HI countries, climate accounts for 96.8% of the exposure increase under SSP245 and 106.7% under SSP585, while cropland effects remain minimal. Conversely, LI and LMI countries experience a greater relative contribution from cropland and interaction effects under SSP245, but as climate change intensifies under SSP585, these contributions decline significantly, reinforcing climate's dominance and leaving low-income regions more exposed to extreme droughts with limited adaptation capacity. UMI countries show a unique trend, with climate's contribution exceptionally high under SSP245 (156.4%), while cropland reduces exposure (-45.6%), but this mitigating effect disappears under SSP585, emphasizing how land-

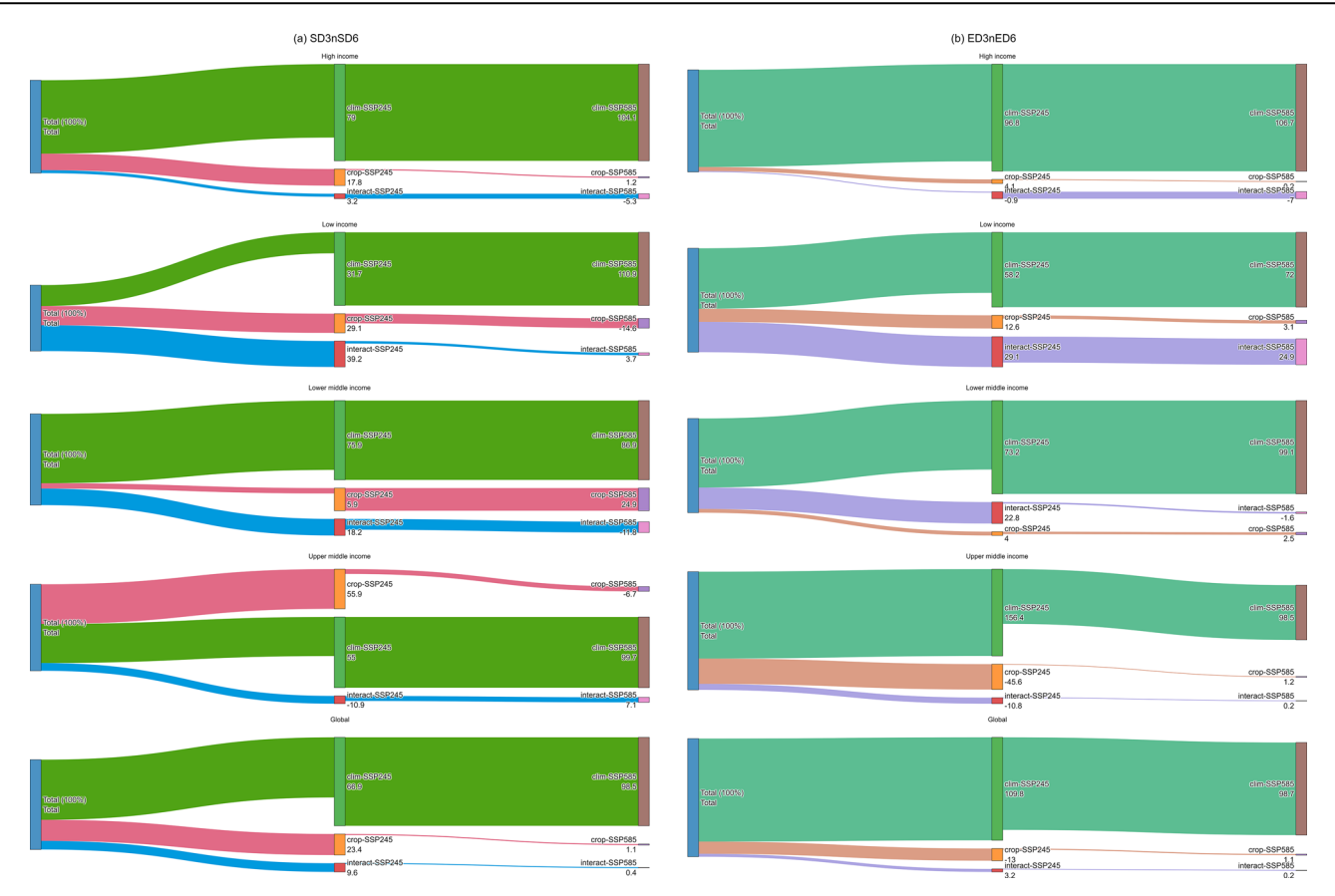


Fig. 9 | Relative contributions of climate change, cropland expansion, and their interaction to cropland exposure under SPI-based 3-month and 6-month. a severe and b extreme droughts.

use patterns may fail to counteract worsening drought conditions in a highemission scenario.

The cropland exposure changes to SPEI-based droughts (Fig. 6) highlight significant increases in exposure to both severe and extreme drought concurrence, with particularly large disparities across income groups. Figure 10 presents the relative contributions to cropland exposure changes to SPEI-based drought concurrences (i.e., SD3nSD6 and ED3nED6). Globally, climate contributes 136.3% to SD3nSD6 under SSP245 and 84.6% under SSP585, while cropland variations exhibit a negative contribution under SSP245 (-92.1%) but become slightly positive (7.0%) under SSP585, indicating that land-use changes offset climate-driven increases under moderate emissions but have little impact under high emissions. For ED3nED6, the role of climate is even stronger, contributing 85.0% under SSP245 and rising to 103.5% under SSP585, whereas cropland's influence is minimal and even negative at the global level (-0.4%)under SSP585, highlighting that land-use changes do not mitigate the intensifying risk of extreme drought concurrence under high-emission scenarios.

Across different income groups, both scenarios reveal significant disparities in the drivers of cropland exposure to drought risks. High-income (HI) countries are overwhelmingly climate-driven, with climate contributing 87.3% to SD3nSD6 under SSP245 and 105.3% under SSP585, while cropland and interaction effects remain minimal or negative. Lower-income (LI) and LMI countries show a more mixed influence under SSP245, where cropland contributes 45.2% (LI) and 27.1% (LMI), while interaction effects contribute 15.6% and 21.2%, respectively, indicating that land-use changes amplify drought exposure in these regions. However, under SSP585, cropland's role increases further in LI (62.7%) and LMI (35.1%) countries for SD3nSD6, whereas interaction effects remain substantial in LMI countries (31.8%) but decline sharply in LI countries (—12.1%), reinforcing climate's increasing dominance overland-use factors. UMI countries exhibit a unique

pattern, where cropland changes strongly counteract climate effects under SSP245 (-201.4% for SD3nSD6), but this mitigation effect disappears under SSP585, with cropland contributing 10.4% and climate remaining dominant at 80.3%. For ED3nED6, the dominance of climate change is evident across all income groups, but its influence strengthens under SSP585, leaving cropland changes with a minimal or even negative impact. In HI countries, climate contributes 91.6% under SSP245 and increases to 105.6% under SSP585, while cropland and interaction effects remain negligible. In LI and LMI countries, interaction effects play a significant role under SSP245 (27.8% and 26.3%, respectively), but decline under SSP585, reinforcing that climate-driven evapotranspiration increasingly dictates extreme drought exposure, particularly in lower-income regions. In UMI countries, climate's contribution rises from 88.2% under SSP245 to 103.1% under SSP585, while cropland contributions and interaction effects become negative under SSP585, further confirming the reduced influence of land-use changes in mitigating drought risks under high-emission scenarios.

As shown in Fig. 7, there are visible increases in cropland exposures to 3-month severe or extreme droughts transitioning into 6-month extreme droughts (i.e., SD3toED6, ED3toED6), with global increases of \sim 30% and \sim 75% for SD3toED6 under SSP245 and SSP585, respectively, and \sim 8% and \sim 38% for ED3toED6. The contributions from climate change, cropland variation and their interactions are presented in Fig. 11. Globally, climate contributes 105.6% to SD3toED6 under SSP245 and 101.4% under SSP585, while cropland variations exhibit a negative contribution under SSP245 (-10.7%) but turn slightly positive under SSP585 (1.2%), indicating that land-use changes offset climate-driven exposure under moderate emissions but have little impact under high emissions. For ED3toED6, climate's role is even stronger, contributing 78.7% under SSP245 and increasing to 111.7% under SSP585, while cropland contributions are minimal and even negative at the global level (-7.1%) under SSP585, reinforcing that land-use changes

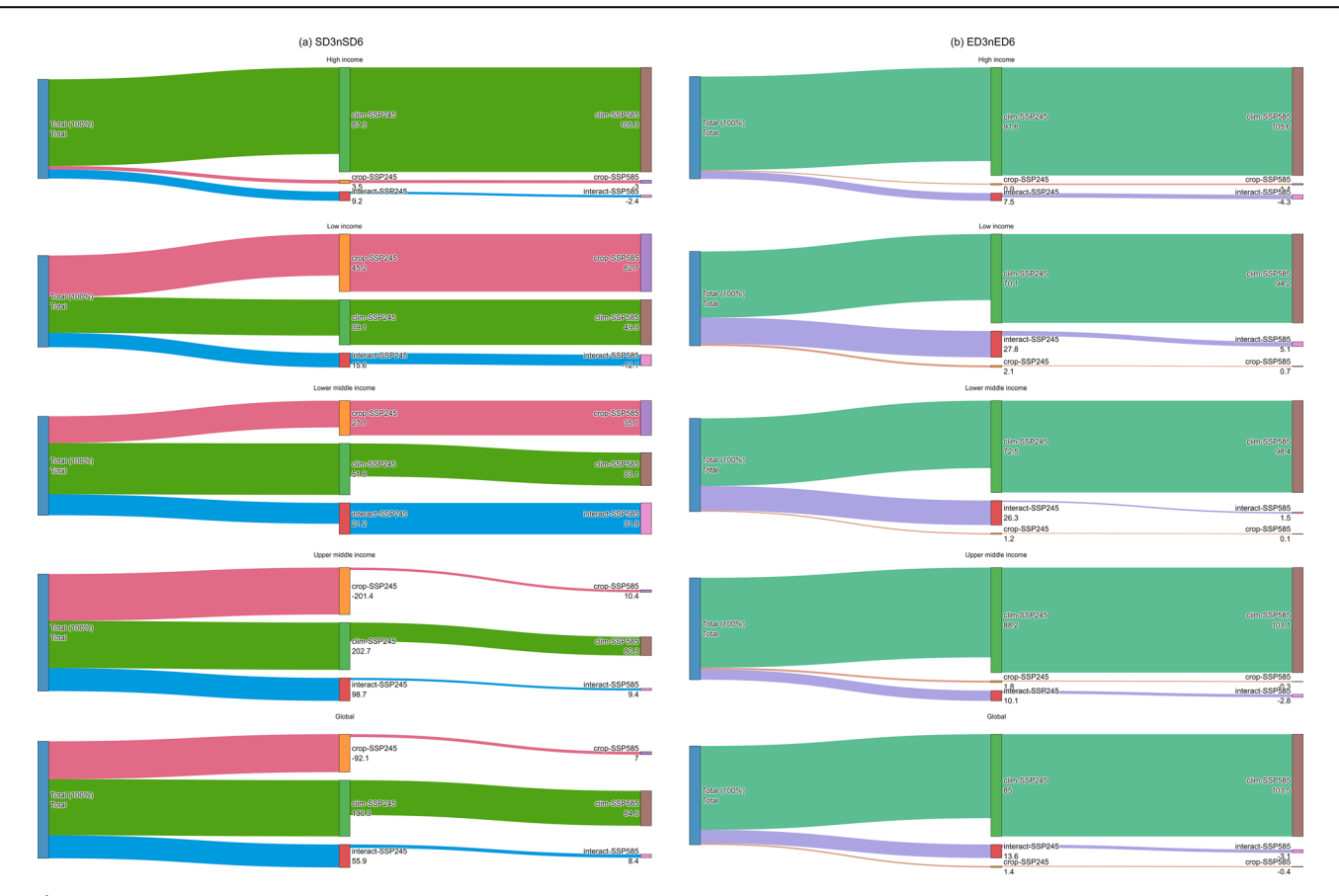


Fig. 10 | Relative contributions of climate change, cropland expansion, and their interaction to cropland exposure under SPEI-based 3-month and 6-month. a severe and b extreme droughts.

do not mitigate the intensifying risk of extreme drought persistence under high-emission scenarios.

Across different income groups, there are significant disparities in the relative contributions of climate, cropland, and their interactions to cropland exposure risks. In high-income (HI) countries, climate remains the overwhelming driver under both SSP245 and SSP585, contributing 147.8% and 113.2% to SD3toED6 and 116.2% and 101.0% to ED3toED6, respectively. Cropland variations have a significant negative contribution (-49.7%) only for SD3toED6 under SSP245, while their influence is negligible (<10%) for all other cases. In contrast, low-income (LI) countries show a more balanced contribution under SSP245, with cropland accounting for 80.8% and 36.1% for SD3toED6 and ED3toED6, respectively, highlighting the role of agricultural expansion in shaping drought exposure. However, under SSP585, cropland's contribution declines (47.6% and 17.6%, respectively), while climate's influence strengthens, reinforcing that extreme drought exposure in LI countries becomes increasingly climate-driven. LMI countries exhibit a similar pattern, with climate contributing 79.9 and 71.4% under SSP245 and rising to 91.7% and 104.3% under SSP585 for SD3toED6 and ED3toED6, respectively, while cropland contributions remain minimal, further emphasizing climate's growing dominance. UMI countries exhibit a distinct shift, where cropland changes significantly counteract climate effects for SD3toED6 under SSP245 (-17.1%), but this mitigation effect disappears under SSP585, with cropland contributing a slightly positive 3.4%. In contrast, cropland variations have a substantial positive effect (24.3%) on ED3toED6 under SSP245, but under SSP585, they instead counteract climate effects, contributing a negative effect of -30.3%.

The cropland exposure to SPEI-based drought transitions into 6-month extreme droughts (SD3toED6 and ED3toED6) follows a similar pattern to SPI-based drought transitions, with substantial increases in exposure across all income groups. Globally, cropland exposure increases by

~250% and ~350% for SD3toED6 under SSP245 and SSP585, and by ~240% and ~320% for ED3toED6, reinforcing the critical role of temperature-driven evapotranspiration in intensifying drought persistence. The contributions from climate change, cropland variations, and their interactions (Fig. 12) reveal notable differences across income groups and between SSP245 and SSP585. Climate change contributes the most to these increases, accounting for 89.7 and 105.3% of SD3toED6 under SSP245 and SSP585, respectively, and 96.8 and 106.1% of ED3toED6, highlighting the growing dominance of climate as emissions increase. Cropland variations, in contrast, exhibit mostly minor but negative contributions (~7.5% for ED3toED6 under SSP245, ~7.6% for SD3toED6, and ~3.3% for ED3toED6 under SSP585), with the exception of SD3toED6 under SSP245 (2.2%), suggesting that land-use changes provide limited mitigation, particularly for 3-month extreme droughts transitioning into 6-month extreme droughts.

The contributions of climate, cropland, and their interactions to cropland exposure risks vary across income groups, highlighting growing disparities in drought vulnerability. In high-income (HI) countries, climate is the dominant driver, contributing over 77.5% to SD3toED6 and 92.9% to ED3toED6 under SSP245, increasing further higher than 100% under SSP585, while cropland effects remain minimal or negative. In LI countries, cropland plays a significant role in SD3toED6 exposure under SSP245, contributing 23.9%, while climate remains the dominant driver at 53.7%. However, under SSP585, cropland's contribution turns highly negative (-159.4%), indicating that land-use changes counteract climate-driven exposure increases, while climate's role intensifies sharply, rising to 153.6%. Meanwhile for ED3toED6, climate remains the dominant driver but with a slight reduction (from 67.0% under SSP245 to 52.0% under SSP585), mainly due to increased contributions from cropland variations (from 5.0% under SSP245 to 37.1% under SSP585), a larger role in modifying extreme drought exposure. LMI countries exhibit a relatively balanced contribution under SSP245, with cropland and interaction effects collectively accounting for

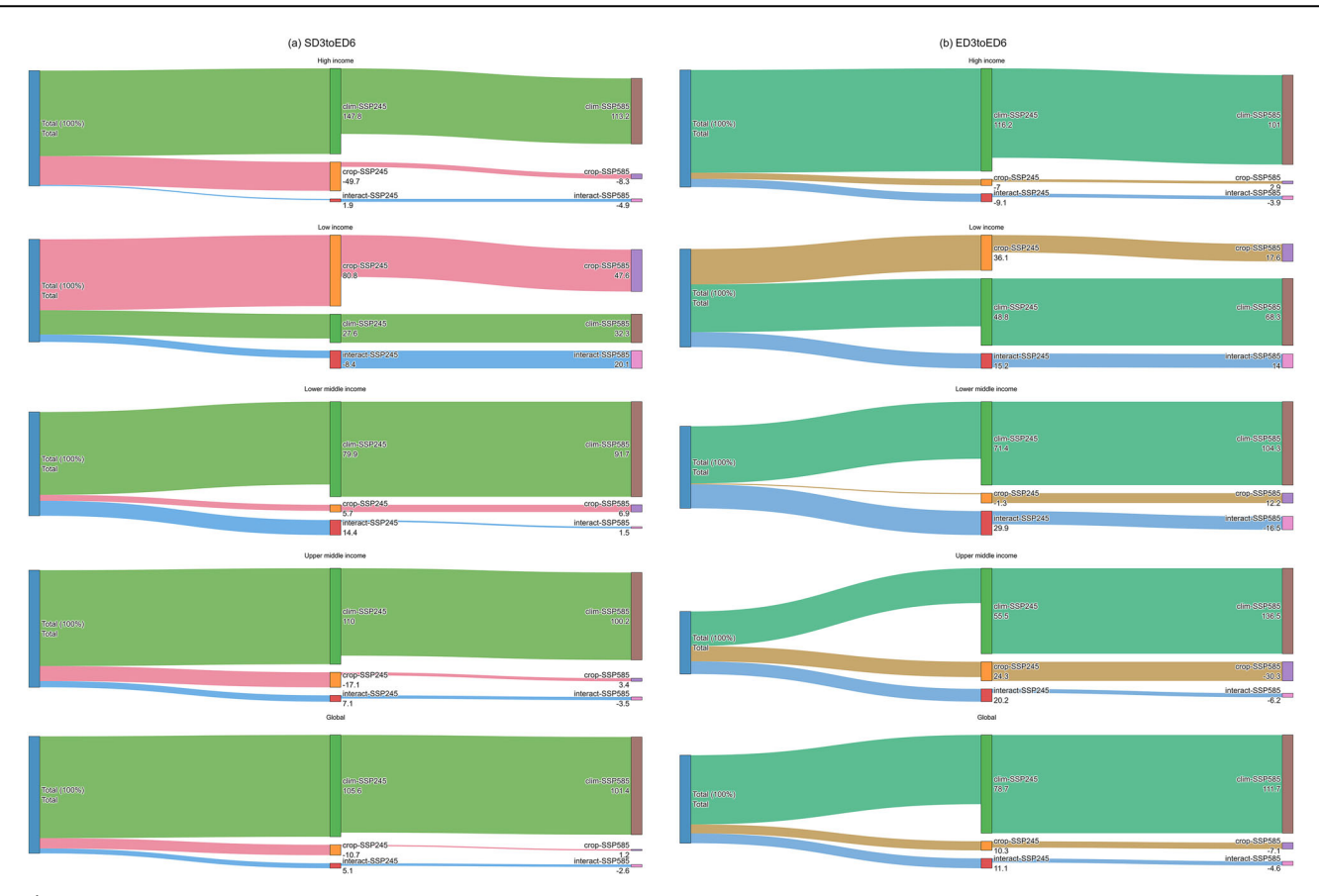


Fig. 11 | Contributions of climate change, cropland expansion, and their interaction to cropland exposure under SPI-based transitional droughts. a 3-month severe drought evolving into a 6-month extreme drought, and b 3-month extreme drought evolving into a 6-month extreme drought.

over 20%. However, under SSP585, climate's dominance increases significantly (96.1% for SD3toED6, 114.4% for ED3toED6), while cropland's influence diminishes or turns negative. UMI countries experience a distinct transition, where cropland mitigates climate-driven exposure under SSP245 (-15.4% for SD3toED6, -30.5% for ED3toED6), but this effect disappears in SSP585, leaving climate as the overwhelming driver.

In general, future cropland exposure to both concurrent (SD3nSD6, ED3nED6) and transitional (SD3toED6, ED3toED6) drought risks is increasingly dominated by climate change, with its influence strengthening under SSP585 across all income groups. High-income countries remain overwhelmingly climate-driven, while low-income countries experience a shift from mixed climate-cropland influences under SSP245 to near-total climate dependence under SSP585, as land-use changes become ineffective or even counteract exposure increases. LMI and UMI countries show diminishing cropland contributions under SSP585, reinforcing growing disparities in drought vulnerability, where lower-income regions face intensified climate-driven risks with limited adaptation potential through land-use strategies.

Uncertainty analysis

In this study, four parametric copulas as well as the independence copula were adopted to model the interdependence among the 3-month and 6-month drought indicators, with the selected copulas being identified by the AIC criteria. The frequency of selected copulas, as well as the distributions of Akaike Information Criterion (AIC) and Kolmogorov-Smirnov (K-S) statistics, for both SPEI and SPI-based drought indicators are presented in Fig. S2.

For SPEI (Fig. S4a-c), the Gaussian copula was most frequently selected (~35%), followed by the Gumbel copula, while a notable proportion of grid cells (~25%) exhibited weak dependence and were assigned the independence copula. The distributions of AIC values (panel b) are left-

skewed, indicating relatively strong fit for the selected copulas, and the majority of K-S statistics (panel c) are concentrated below 0.1, suggesting satisfactory goodness-of-fit across most regions. For SPI (Fig. S2d-f), a larger number of grid cells (~50%) exhibited weak dependence and were assigned the independence copula, reflecting the weaker correlation structure between SPI-3 and SPI-6 at these locations. However, where dependence exists, Gaussian and Gumbel copulas were again predominantly selected. The AIC and K-S distributions (panels e and f) are consistent with those observed for SPEI, reinforcing the robustness of the selected copula structures. The choice of copula significantly influences the joint tail behavior and hence the estimated risks of compound drought events. By using a data-driven selection process that minimizes AIC and passes K-S tests, our approach ensures that the copula structure at each grid cell is optimally chosen to reflect local dependence characteristics.

In addition to spatial variations in copula models across grid cells, substantial uncertainties also exist in projecting cropland exposure to compound drought events, arising from multiple sources such as variability across GCMs, the choice of drought indicators (SPI vs. SPEI), and PET estimation methods. Figures S3 and S4 present the model spread across 12 GCMs for SPI- and SPEI-based exposure estimates. These plots reveal substantial inter-model variation, particularly under the SSP585 scenario, for cropland exposures to 3-month and 6-month extreme drought events (ED3nED6), as well as transitions from 3-month severe or extreme drought to 6-month extreme drought (SD3toED6 and ED3toED6, respectively).

As presented in Figs. S5 and S6, among all the drought risk indicators considered, the transitions involving extreme drought events—namely ED3nED6, SD3toED6, and ED3toED6—consistently exhibit the largest uncertainty ranges. This is evident for cropland exposures to both SPI and SPEI-droughts. For example, in SPEI-based projections for ED3nED6 (Fig. S4d), the projected change rate in cropland exposure shows extensive ranges from –4000% to over +125,00% for a global scale under SSP585, with

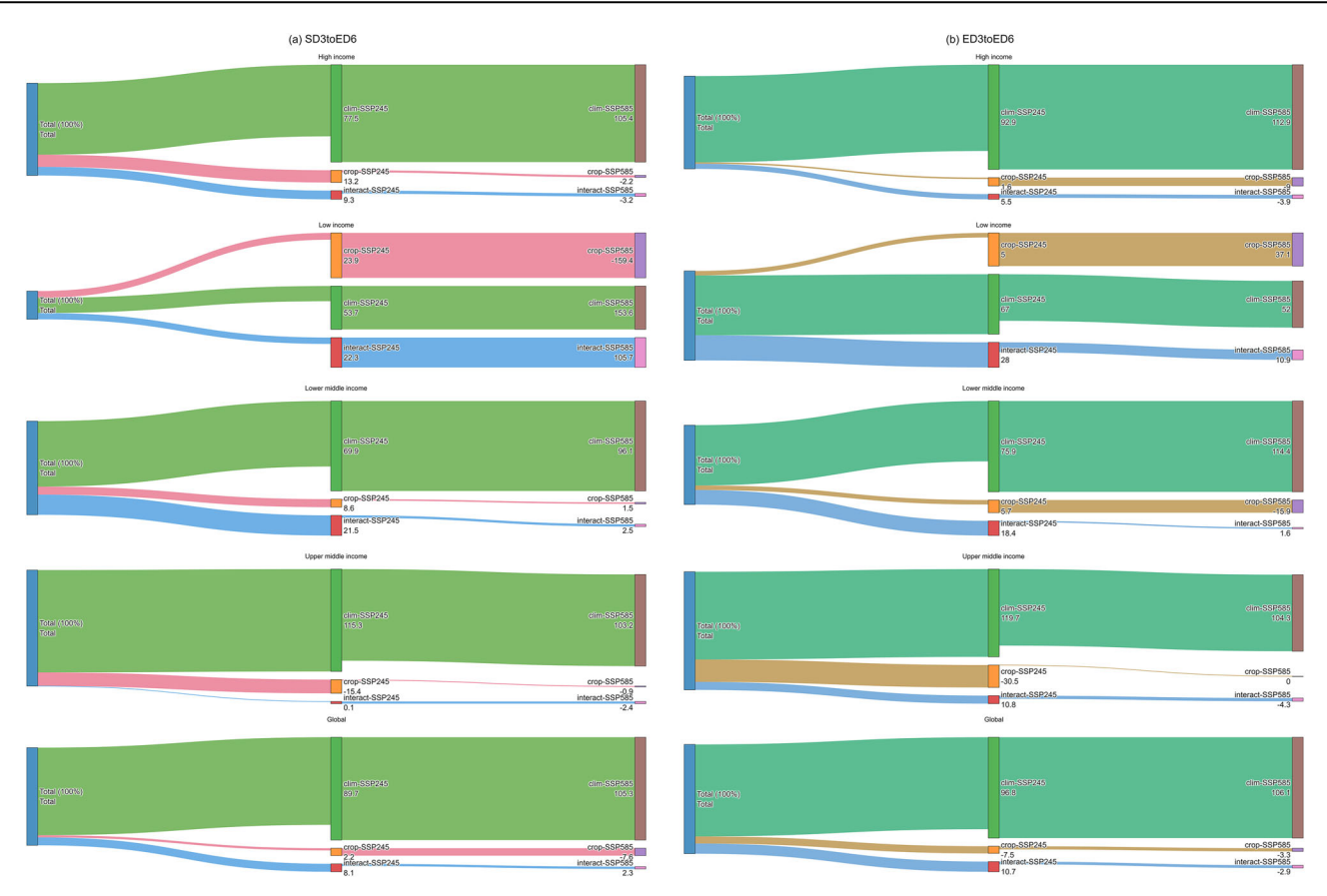


Fig. 12 | Contributions of climate change, cropland expansion, and their interaction to cropland exposure under SPEI-based transitional droughts. a 3-month severe drought evolving into a 6-month extreme drought, and b 3-month extreme drought evolving into a 6-month extreme drought.

a median around +3500%. Similarly, for ED3toED6 (Fig. S4f), the spread spans from approximately -200% to +400%. This high variability reflects both the complexity of compound drought definitions and their sensitivity to inter-model climate differences.

Moreover, for both SPI- and SPEI-based estimates, the SSP585 scenario generally exhibits greater uncertainty than SSP245, especially for transitions to multi-month extreme drought. In SPI-based ED3nED6 projections (Fig. S3d), SSP585 shows a broader range—from roughly 0% to +12.50%—compared to SSP245, which is more tightly clustered around -100–400% in a global scale. This pattern persists across income groups and drought types involving extreme drought indicators, highlighting the greater divergence among climate model projections under high-emission scenarios.

Furthermore, compared to SPI-based cropland exposures, SPEI-based exposure estimates show significantly wider spreads, indicating greater overall uncertainty. This difference arises primarily from the inclusion of PET in SPEI, which introduces additional sources of variability due to differing GCM representations of radiation, humidity, and wind. For instance, under SD3toED6 transitions, the median exposure change in a global scale under SPEI (Fig. S4c) exceeds +250% with a range of [-200,700]%, compared to about +100% (ranges from -50 to 200%) for SPI (Fig. S3c). Across all transitions and income levels, the interquartile ranges are consistently wider for SPEI, with particularly large spreads in lowincome (LI) and high-income (HI) regions.

Besides uncertainties arising from GCM projections and the choice of drought indicators, SPEI-based drought risks are also affected by the method used to estimate PET. Figure S7 illustrates the uncertainties in cropland exposure to SPEI-based drought risks when PET is estimated using the Hargreaves method. Consistent with earlier findings based on the Penman–Monteith (PM) approach, the largest uncertainties are observed for drought indicators involving extreme conditions over longer durations

-specifically ED3nED6, SD3toED6, and ED3toED6. These indicators exhibit broader interquartile ranges and higher upper bounds, particularly under the SSP585 scenario. Notably, SSP585 consistently produces wider spreads and higher median exposure rates across most income groups compared to SSP245, reflecting greater inter-model divergence under highemission pathways. Compared to the Penman-Monteith-derived PET, the use of the Hargreaves method substantially narrows the spread of cropland exposure changes. This reduction in variability stems from the simplified input requirements of the Hargreaves method, which only relies on temperature data. In contrast, the Penman-Monteith method incorporates additional variables such as humidity, solar radiation, and wind speedeach of which introduces its own uncertainties. These compound uncertainties in input data propagate through the PET estimation process and amplify the overall uncertainty in drought risk assessments and associated cropland exposures. However, compared to the SPI-based cropland exposures shown in Fig. S3, the SPEI-based exposures using PET from the Hargreaves method still exhibit greater uncertainty. This indicates that while the choice of PET formulation contributes significantly to overall uncertainty, it does not change the overarching conclusions: (i) the SPEIbased drought risk projections consistently display higher variability than SPI-based ones, (ii) exposures to compound extreme droughts are particularly uncertain, and (iii) these uncertainties are most pronounced under high-emission scenarios.

Discussion

This study presents a comprehensive global assessment of future cropland exposure to drought risks under climate change, focusing on the relative contributions of climate variability and land-use changes across different income groups. We analyzed concurrent 3-month and 6-month drought risks during key crop-growing periods using the Standardized Precipitation Index (SPI) and the SSPEI, employing a copula-based approach to capture

joint drought occurrences. Additionally, we assessed transitional risks, examining the probability of 3-month droughts evolving into 6-month droughts. By integrating high-resolution global cropland data, we evaluated cropland exposure to both concurrent and transitional drought risks under SSP245 and SSP585 scenarios, identifying disparities across income groups and quantifying the dominant drivers of exposure changes.

The results reveal distinct patterns in future drought risks across drought indices and climate scenarios. SPI-based concurrent 3-month and 6-month severe droughts (SD3nSD6) show minimal changes under SSP245 and SSP585, with percentage shifts mostly within [-1, 1]. SPEI-based SD3nSD6 shows slight increases, remaining under 5 percentage points. In contrast, extreme drought concurrence (ED3nED6) increases notably, with SPI-based projections showing up to 10 percentage point rises in parts of Europe and South America under SSP585. SPEI-based ED3nED6 highlights more severe increases, with northwestern China, Europe, northern Africa, and the Arabian Peninsula seeing up to 20 percentage point rises under SSP245, and over 60% under SSP585. Drought transitions further emphasize risk disparities, as both indices show rising probabilities of 3-month droughts evolving into 6-month extreme droughts (SD3toED6, ED3toED6), with SPEI-based results revealing transition risk increases exceeding 50 percentage points, driven by temperature-induced evapotranspiration.

The results highlight the escalating threat of future droughts to global croplands, with exposure risks varying across drought types, scenarios, and income groups. SPI-based severe droughts (SD3nSD6) show moderate cropland exposure increases (~12.5% under SSP585), while extreme droughts (ED3nED6) double under SSP245 and quadruple under SSP585. LMI countries face the highest increases (>350%), while high-income (HI) countries see the lowest (~250%). SPEI-based projections reveal greater impacts due to temperature-driven evapotranspiration, with SD3nSD6 exposure more than doubling and ED3nED6 surging by 2000% under SSP245 and 4200% under SSP585, especially affecting LMI countries (>5000%). Drought transitions further amplify vulnerabilities, with SPIbased SD3toED6 exposure rising by 30% under SSP245 and 75% under SSP585, and SPEI-based transitions increasing by 250% and 350%, respectively. Income-based disparities widen under SSP585, with LMI countries facing the most severe relative risks, emphasizing the need for targeted adaptation and climate mitigation strategies.

Cropland exposure to future drought risks is primarily driven by climate change, with its influence intensifying under high-emission scenarios (SSP585), where contributions often exceed 100%, minimizing the role of land-use changes. For SPI-based severe droughts (SD3nSD6), climate accounts for ~67% of exposure increases under SSP245, rising to ~98.5% under SSP585. Extreme droughts (ED3nED6) show similar trends, with global exposure doubling under SSP245 and quadrupling under SSP585, predominantly climate-driven. SPEI-based projections further highlight the amplifying effect of temperature-driven evapotranspiration, especially for drought transitions. While cropland and interaction effects moderately impact lower-income regions under SSP245, climate dominance overshadows these under SSP585. In high-income countries, climate remains the primary driver, while in low-income regions, land-use changes initially play a role but diminish or become negative under SSP585.

This study advances understanding of global cropland vulnerability to future droughts by integrating climate extremes, land-use dynamics, and socioeconomic disparities. It integrates multi-timescale drought analysis with a copula-based approach using SPI and SPEI indices to assess both concurrent and transitional drought risks, while capturing the amplifying impact of temperature-driven evapotranspiration. The study highlights how high-emission scenarios exacerbate drought exposure, disproportionately impacting lower-income regions, and identifies climate change as the primary driver of future risks. These findings provide critical insights for targeted adaptation strategies and sustainable agricultural planning under climate change.

While this study offers a globally consistent assessment of cropland exposure to compound drought risks, several limitations still exist. Although

we applied a rigorous data-driven procedure for copula selection based on AIC and K-S tests, we did not quantify the uncertainty surrounding the copula dependence parameters themselves. Techniques such as bootstrapping or sensitivity analysis could help in this regard; however, their application at a global scale is computationally prohibitive under current constraints. Moreover, the 3-month and 6-month SPI and SPEI indicators provides a broad approximation of drought persistence across crop-growing seasons, but local cropping calendars and hydrological responses may vary significantly and require regional-scale refinement. While we incorporated multiple GCMs and PET estimation methods to assess inter-model uncertainty, we did not explicitly address structural uncertainties in landuse projections or adaptation responses. In addition, the analysis of exposure disparities by income group relies on fixed income classifications from the World Bank in 2020. Particularly for the LMI category, which encompasses countries with highly heterogeneous climates, agricultural systems, and adaptive capacities, our grouping may obscure important regional differences. Furthermore, income levels are dynamic and may shift by the end of the century, which could alter interpretations of long-term exposure trends. Consequently, future work should consider probabilistic frameworks and ensemble-based decision tools that integrate uncertainty propagation from climate, land-use, socioeconomic dynamics, and model structure to better inform drought resilience strategies.

Methods

Data on climate projection and cropland expansion

In this research, we leveraged climate simulations and projections from 12 GCM models (see Table 1) within the Coupled Model Intercomparison Project Phase 6 (CMIP6) to evaluate drought conditions under two specific Shared Socioeconomic Pathways (SSP245 and SSP585). These selected models encompass a wide range of geographical sources and spatial resolutions, providing a thorough assessment of how projected climate changes might influence the severity and frequency of droughts. The selection of GCMs was guided by recent empirical studies, which highlight the critical role of model accuracy in simulating key climate variables such as precipitation and temperature—essential components for reliable drought analysis²⁵⁻³¹. Moreover, this study specifically focuses on assessing future drought risks under the SSP245 and SSP585 scenarios. SSP245 represents a scenario where socio-economic trends mirror historical patterns, leading to an intermediate level of radiative forcing by the end of the century, approximately 4.5 W/m², aiming to moderate climate warming³². In contrast, SSP585 outlines a "Fossil-Fueled Development" future, characterized by high energy demand and continued reliance on fossil fuels, resulting in the highest greenhouse gas emissions among the SSP scenarios, with radiative forcing exceeding 8.5 W/m² by 2100³³.

Table 1 | CMIP6 climate models used in this study

ID	Model	Country	Resolution
1	ACCESS-CM2	Australia	2.8° × 2.8°
2	ACCESS-ESM1-5	Australia	2.8° × 2.8°
3	CMCC-CM2-SR5	Italy	1.25° × 0.9°
4	EC-Earth3	Spain	100 km
5	GFDL-ESM4	US	100 km
6	INM-CM4-8	Russia	1.4° × 1.4°
7	INM-CM5-0	Russia	1.4° × 1.4°
8	IPSL-CM6A-LR	France	2° × 1.5°
9	MIROC6	Japan	2.5° × 1.3°
10	MPI-ESM1-2-HR	Germany	250 km
11	MPI-ESM1-2-LR	Germany	250 km
12	MRI-ESM2-0	Germany	250 km

All model outputs were regridded to a common resolution of 250 km (matching MRI-ESM2-0) prior to analysis.

Monthly precipitation data for both historical (1951-2010) and future (2041-2100) periods were obtained from the World Climate Research Programme (WCRP) (https://esgf-node.llnl.gov/search/cmip6/). These datasets enable an analysis of changes in the SPI across both historical and projected future timeframes. Additionally, PET data are required to compute the SPEI, which can be derived through various methods using meteorological variables. For this research, PET data were sourced from Bjarke et al.34, who provided global monthly estimates using the Penman-Monteith method, based on climate projections from multiple GCMs in CMIP6^{34,35}. The PET dataset from Bjarke et al. ^{34,35} aligns well with estimates from the Climate Research Unit (CRU) and the ERA5-Land reanalysis dataset, confirming its suitability for use in this analysis. Moreover, the multi-model ensemble (MME) was adopted in this study, with each model assigned equal weights. Figure S1 illustrates the performance of each model in simulating precipitation and PET compared to observations from the CUR dataset. The results show substantial variability among individual models. However, the MME consistently exhibits strong performance, with its position located near the observational reference point in both diagrams. This supports the long-standing finding that MME approaches can effectively reduce random errors and compensate for individual model biases

The cropland data for both historical and future periods were sourced from Cao et al. 36, who developed a global cropland proportion dataset at a 1-km resolution spanning from 10,000 BCE to 2100 CE using a harmonization and downscaling framework. This high-resolution dataset offers a detailed view of cropland distribution and spatial heterogeneity. In this study, cropland areas are not merely upscaled to match the resolution of the GCM outputs. Instead, we calculate the cropland areas within each GCM grid cell individually for both historical and future periods. Specifically, for each GCM grid cell, we first identify the corresponding 1-km resolution grids from the cropland dataset located within that cell. We then calculate the cropland area for each 1-km grid and sum these to determine the total cropland area within the GCM grid cell.

Drought indicators

There are numerous metrics used to diagnose drought globally, with the SPI and the SPEI being two of the most widely utilized drought indices 10,11 . The SPI focuses solely on precipitation anomalies, making it useful for assessing drought in areas where temperature has a minimal effect on water demand. It is calculated by fitting the precipitation data to a probability distribution, often the gamma distribution, and transforming it into a standard normal distribution 10 . In contrast, SPEI accounts not only for precipitation but also for PET, which reflects the effect of temperature on drought conditions. SPEI is based on a water balance model where PET is subtracted from precipitation, and the resulting difference is fitted to a log-logistic distribution 11 . The formula for SPEI is similar to SPI, with the water balance D = P - PET replacing precipitation in the calculation 37 .

Based on either SPI or SPEI, drought severity can be categorized into different levels such as moderate, severe, and extreme drought. The specific SPI/SPEI thresholds for these severity levels are outlined in Table 2. In this study, we will primarily focus on assessing the risks of severe and extreme droughts under different climate change scenarios. To better understand the potential impact of drought on future agriculture, we will analyze drought risks during the 3-month and 6-month periods that cover the main growing seasons for crops. In the Northern Hemisphere (NH), the 3-month period

Table 2 | Drought severity using SPI/SPEI indices9

Drought severity levels	SPI/SPEI value
No drought	SPI/SPEI > -1
Moderate drought	-1.0 ≥ SPI/SPEI > -1.5
Severe drought	-1.5 ≥ SPI/SPEI > -2.0
Extreme drought	-2.0 ≥ SPI/SPEI

corresponds to April–June and the 6-month period to April–September. In the Southern Hemisphere (SH), the corresponding 3-month and 6-month periods are October–December and October–March, respectively. These time scales are widely used in agroclimatic studies and align with typical planting-to-harvest durations for major crops worldwide. While the growing seasons vary across regions—for example, lasting only 3–4 months in northern areas such as Canada or Scandinavia, and longer in tropical or subtropical zones—our choice of 3- and 6-month periods aims to provide a globally consistent basis for analyzing drought persistence risks. For regional applications, local crop calendars and climate characteristics would need to be taken into account to refine this framework.

Drought occurrence and transition risks

This study aims to characterize drought evolution over periods ranging from 3 to 6 months, encompassing the primary crop-growing seasons. The 3-month and 6-month SPI/SPEI indicators are likely to be correlated, as the 6-month accumulation inherently includes the preceding 3 months. Also, the goal of our analysis is not to treat them as orthogonal variables, but rather to assess the persistence and transitions of drought conditions over agriculturally meaningful time scales. The 3-month drought captures earlyseason deficits, while the 6-month drought reflects extended water stress that can affect crop yield. To achieve this, the copula method was applied to quantify the interdependence between 3-month and 6-month drought events. Over the last two decades, the copula method has been widely used to model and analyze the dependence structure between different variables in various fields, including hydrology, climatology, and agriculture. Its ability to capture non-linear and asymmetric relationships has made the copula method particularly valuable for studying complex environmental phenomena, such as droughts, floods, and other hydroclimatic hazards, within a multivariate context. This has greatly enhanced our understanding of their underlying dynamics and their impacts on both natural and human systems.

For either SPI or SPEI with 3-month and 6-month time scales respectively denoted as X_{3mon} and X_{6mom} the interdependence between these two drought index values can be described by the copula function as follows:

$$F(x_{3mon}, x_{6mon}) = C_{\theta}(F_{3mon}(x_{3mon}), F_{6mon}(x_{6mon})) \tag{1}$$

where $F_{3mon}(x)$ and $F_{6mon}(x)$ represents the marginal distributions for X_{3mon} and X_{6mon} , respectively; C_{θ} is the copula function with a parameter set of θ . In this study, the empirical marginal distributions are adopted for X_{3mon} and X_{6mon} , whilst parametric copula functions including Gaussian, Gumbel, Frank, and Joe copulas, were used to model their interdependence. There have been studies using empirical copulas to model multivariate characteristics in drought risk analysis $^{38-40}$. However, parametric copulas offer distinct advantages in the current study as there are a variety of parametric copulas available, allowing flexibility in modeling dependence structures.

The copula modeling procedure consists of the following steps:

- 1. Dependence Assessment: For each grid cell, the correlation between historical X3mon and X6mon drought indicators is evaluated using Kendall's τ . If a statistically significant dependence is detected, parametric copulas are considered for modeling. Otherwise, an independence copula is used.
- 2. Copula Selection: For grid cells with significant dependence, Gaussian, Gumbel, Frank, and Joe copulas are fitted to the data. The selection of the optimal copula is based on two criteria: (a) passing the Kolmogorov-Smirnov (K-S) goodness-of-fit test, and (b) achieving the lowest Akaike Information Criterion (AIC) score. The selected copula is then used for subsequent compound drought risk analysis.
- 3. Application to Future Periods: Given that copula structure has a notable influence on estimates of compound extremes^{41,42}, we maintain the same copula family selected during the historical period for future simulations. However, the copula parameter is re-estimated based on future drought indicator time series. This ensures consistency in dependence structure modeling while adapting to changing marginal behaviors.

The use of parametric copulas in this context offers several key strengths. They enable flexible modeling of nonlinear dependence beyond linear correlation, which is essential for characterizing compound droughts spanning different time scales. Moreover, their computational efficiency makes them particularly suitable for global applications involving highresolution grids and large datasets. Nevertheless, several limitations should be acknowledged. Firstly, parametric copulas rely on assumed functional forms—often with symmetric or asymmetric tail behavior—which may not fully reflect localized or complex dependence structures. Secondly, the results are sensitive to the choice of both the copula family and the fitted marginal distributions, which may affect the accuracy of joint extremes. Finally, although non-parametric or semi-parametric alternatives offer greater flexibility, they are computationally intensive and not practical for global-scale analyses. To address these limitations, we implemented a robust model selection framework combining the AIC and K-S test at each grid cell. This ensures that the selected copula strikes a balance between statistical performance and computational feasibility, thereby supporting a consistent and scalable analysis of compound drought risk across diverse climatic and geographic regions.

In this study, the frequencies of 3-month and 6-month severe drought (SD) and extreme drought (ED) under different climate conditions will be analyzed using both SPI and SPEI. Utilizing the copula model described in Eq. (1), the joint probabilities of 3-month and 6-month droughts, for either SPI or SPEI, can be effectively quantified, enabling a comprehensive understanding of their interdependence. Refer to the drought severity categories in Table 2, the concurrence risk severe drought (SD3nSD6) and extreme drought (ED3nED6) can be expressed as follows:

$$\begin{split} \mathbf{P}_{SD3nSD6} &= C_{\theta}(F_{3mon}(-2.0 < x_{3mon} \le -1.5), F_{6mon}(-2.0 < x_{6mon} \le -1.5)) \\ &= C_{\theta}(F_{3mon}(-1.5), F_{6mon}(-1.5)) - C_{\theta}(F_{3mon}(-2.0), F_{6mon}(-1.5)) \\ &- C_{\theta}(F_{3mon}(-1.5), F_{6mon}(-2.0)) \\ &+ C_{\theta}(F_{3mon}(-2.0), F_{6mon}(-2.0)) \end{split} \tag{2}$$

$$P_{ED3nED6} = C_{\theta}(F_{3mon}(x_{3mon} \le -2.0), F_{6mon}(x_{6mon} \le -2.0))$$

$$= C_{\theta}(F_{3mon}(-2.0), F_{6mon}(-2.0))$$
(3)

Furthermore, the copula model developed for the 3-month and 6-month drought indices can also be used to assess the transition risks between different drought conditions, specifically the transitions between severe and extreme droughts, under various future climate scenarios. Understanding these transition risks is essential for evaluating how short-term droughts may escalate into prolonged and more severe conditions. In detail, the transition risks among 3-month and 6-month droughts can be derived as:

(a) 3-month severe drought to 6-month severe drought (SD3toSD6)

$$P_{SD3toSD6} = \Pr\{(x_{6mon} \in SD) | (x_{3mon} \in SD)\}$$

$$= \frac{C_{\theta}(F_{3mon}(-2.0 < x_{3mon} \le -1.5), F_{6mon}(-2.0 < x_{6mon} \le -1.5))}{\Pr\{-2.0 < x_{3mon} \le -1.5\}}$$
(4a)

(b) 3-month severe drought to 6-month extreme drought (SD3toED6)

$$P_{SD3toED6} = Pr\{(x_{6mon} \in ED) | (x_{3mon} \in SD)\}$$

$$= \frac{C_{\theta}(F_{3mon}(-2.0 < x_{3mon} \le -1.5), F_{6mon}(x_{6mon} \le -2.0))}{Pr\{-2.0 < x_{3mon} \le -1.5\}}$$
(4b)

(c) 3-month extreme drought to 6-month severe drought (ED3toSD6)

$$P_{ED3toSD6} = \Pr\{(x_{6mon} \in SD) | (x_{3mon} \in ED)\}$$

$$= \frac{C_{\theta}(F_{3mon}(x_{3mon} \leq -2.0), F_{6mon}(-2.0 < x_{6mon} \leq -1.5))}{\Pr\{x_{3mon} \leq -2.0\}}$$
(4c)

(d) 3-month extreme drought to 6-month extreme drought (ED3toED6)

$$P_{ED3 toED6} = \Pr\{(x_{6mon} \in ED) | (x_{3mon} \in ED)\}$$

$$= \frac{C_{\theta}(F_{3mon}(x_{3mon} \le -2.0), F_{6mon}(x_{6mon} \le -2.0))}{\Pr\{x_{3mon} \le -2.0\}}$$
(4d)

Cropland exposure changes to droughts

The drought-induced cropland exposure is defined as crop-cultivable land situated in areas prone to drought events, which can be quantified by multiplying the estimated drought frequency (DF) by the total cropland area within a drought-prone region. Refer to Mondal et al²³., the cropland exposure can be expressed as:

$$CE_{i,i} = C_i \times F_{i,i} \tag{5}$$

where $CE_{i,j}$ indicates the affected cropland at grid i to hazard j; C_i is the cropland area at grid i, and $F_{i,i}$ is the frequency of drought j at grid i. In this study, drought exposure is defined as the product of cropland area and drought frequency, implicitly assuming that all cropland is equally susceptible to drought. While this simplification does not account for yield gradients or irrigation buffers, the metric remains meaningful for several reasons. First, even in irrigated regions, droughts often lead to increased water demand and irrigation costs, especially where water availability is limited. Thus, drought occurrence still represents a significant stressor, requiring resource allocation for mitigation. From this perspective, the metric can also serve as a proxy for the area requiring potential droughtresponse measures, such as supplemental irrigation. Moreover, our primary objective is not to quantify precise yield losses, but to reveal spatial inequalities in drought exposure under future scenarios. For this purpose, the adopted metric offers a consistent and interpretable indicator across global regions.

Due to climate change and anthropogenic activities, drought-induced cropland exposure is expected to change in the future. These changes will likely be influenced by cropland alterations, climate variability, and the combined effects of cropland and climate interactions²³. Consequently, the cropland exposure changes can be decomposed as:

$$\begin{split} \Delta D &= X_{crop,j} \times X_{cli,j} - X_{crop,i} \times X_{cli,i} = X_{crop,i} \times \Delta X_{cli} + \Delta X_{crop} \times X_{cli,i} \\ &+ \Delta X_{crop} \times \Delta X_{cli} \end{split} \tag{6}$$

where ΔD is the total change in cropland exposure; $X_{crop,i}$ and $X_{crop,j}$ respectively denotes the cropland status (km²) in the time period i and j; $X_{cli,i}$ and $X_{cli,j}$ represents the drought frequency in time period i and j, respectively; ΔX_{crop} is the cropland change from time period i to j; ΔX_{cli} denotes the drought frequency change from time period i to j. In Eq. (6), $X_{crop,i} \times \Delta X_{cli}$ represents the climate change effect, $\Delta X_{crop} \times X_{cli,i}$ denotes the cropland change effect, and $\Delta X_{crop} \times \Delta X_{cli}$ reflect the joint cropland-climate change effect. Consequently, the contribution for each influencing factor can be obtained as:

$$CTR_{crop} = \frac{\Delta X_{crop} \times X_{cli,i}}{X_{crop,i} \times \Delta X_{cli} + \Delta X_{crop} \times X_{cli,i} + \Delta X_{crop} \times \Delta X_{cli}} \times 100\%$$
 (7a)

$$CTR_{cli} = \frac{X_{crop,i} \times \Delta X_{cli}}{X_{crop,i} \times \Delta X_{cli} + \Delta X_{crop} \times X_{cli,i} + \Delta X_{crop} \times \Delta X_{cli}} \times 100\% \quad (7b)$$

$$CTR_{crop-cli} = \frac{\Delta X_{crop} \times \Delta X_{cli}}{X_{crop,i} \times \Delta X_{cli} + \Delta X_{crop} \times X_{cli,i} + \Delta X_{crop} \times \Delta X_{cli}} \times 100\%$$

where CTR_{crop} CTR_{cli} and $CTR_{crop-cli}$ respectively denote the relative contribution from cropland variation, climate change, and interact effect of cropland and climate change. In Equations (7), the contributions of cropland expansion (CTR_{crop}), climate change (CTR_{cli}), and their interaction ($CTR_{crop-cli}$) are calculated using a decomposition approach that allows individual terms to exceed 100% or be negative. Values above 100% indicate that a factor alone drives a change larger than the net total, often due to offsetting effects from other factors. Negative values reflect factors that reduce overall exposure, which is common when one component counteracts the increase driven by another. While each term may fall outside the 0–100% range, their sum always equals the total change in cropland exposure (ΔD), ensuring consistence

Data availability

The CMIP6 simulated data used in the study are available from the Earth System Grid Federation (ESGF) Archive, https://esgf.llnl.gov/. The potential evapotranspiration data derived from CMIP6 projections are available at https://zenodo.org/records/7789759. The monthly observation data are obtained from Climatic Research Unit (CRU) at https://crudata.uea.ac.uk/cru/data/hrg/cru_ts_4.07/.

Code availability

Code used for the analysis is available upon reasonable request.

Received: 26 February 2025; Accepted: 4 September 2025; Published online: 08 October 2025

References

- Godfray, H. C. J. et al. Food security: the challenge of feeding 9 billion people. Science 327, 812–818 (2010).
- Tilman, D., Balzer, C., Hill, J. & Befort, B. L. Global food demand and the sustainable intensification of agriculture. *Proc. Natl. Acad. Sci. USA* 108, 20260–20264 (2011).
- Potapov, P. et al. Global maps of cropland extent and change show accelerated cropland expansion in the twenty-first century. *Nat. Food* 3, 19–28 (2022).
- FAO. Land statistics 2001–2022 Global, regional and country trends. FAOSTAT Analytical Briefs, 88. Rome. https://doi.org/10.4060/ cd1484en (2024).
- van Dijk, M. et al. A meta-analysis of projected global food demand and population at risk of hunger for the period 2010–2050. *Nat. Food* 2, 494–501 (2021).
- Kim, W., Iizumi, T. & Nishimori, M. Global patterns of crop production losses associated with droughts from 1983 to 2009. *J. Appl. Meteorol. Climatol.* https://doi.org/10.1175/JAMC-D-18-0174.1 (2019).
- Brás, T. A., Seixas, J., Carvalhais, N. & Jägermeyr, J. Severity of drought and heatwave crop losses tripled over the last five decades in Europe. Environ. Res. Lett. 16, 065012 (2021).
- AghaKouchak, A. A multivariate approach for persistence-based drought prediction: Application to the 2010–2011 East Africa drought. J. Hydrol. 526, 127–135 (2015).
- Haile, G. G. et al. Projected impacts of climate change on drought patterns over East Africa. Earth's. Future 8, e2020EF001502 (2020).
- McKee, T. B., Doesken, N. J. & Kleist, J. The relationship of drought frequency and duration to time scales. In *Proc. 8th Conference on Applied Climatology* (Anaheim, 1993).

- Vicente-Serrano, S. M., Beguería, S. & López-Moreno, J. I. A multiscalar drought index sensitive to global warming: the standardized precipitation evapotranspiration index. *J. Clim.* 23, 1696–1718 (2010).
- 12. Lehner, F. et al. Projected drought risk in 1.5 °C and 2 °C warmer climates. *Geophys. Res. Lett.* **44**, 7419–7428 (2017).
- Wu H., Su X., Singh V. P., AghaKouchak A. & Liu, Z. Bayesian vine copulas improve agricultural drought prediction for long lead times. *Agric. Forest Meteorol.* 331, https://doi.org/10.1016/j.agrformet. 2023.109326 (2023).
- Chiang, F., Mazdiyasni, O. & AghaKouchak, A. Evidence of anthropogenic impacts on global drought frequency, duration, and intensity. *Nat. Commun.* 12, 2754 (2021).
- Wu, G. et al. Impacts of global climate warming on meteorological and hydrological droughts and their propagations. *Earth's. Future* 10, e2021EF002542 (2022).
- Mohammed, S. et al. Assessing the impacts of agricultural drought (SPI/SPEI) on maize and wheat yields across Hungary. Sci. Rep. 12, 8838 (2022).
- Parsons, D., Rey, D., Tanguy, M. & Holman, I. P. Regional variations in the link between drought indices and reported agricultural impacts of drought. *Agric. Syst.* 173, 119–129 (2019).
- Hamal, K. et al. Assessment of drought impacts on crop yields across Nepal during 1987–2017. Meteorol. Appl. 27, e1950 (2020).
- Peña-Gallardo, M., Vicente-Serrano, S. M., Domínguez-Castro, F. & Beguería, S. The impact of drought on the productivity of two rainfed crops in Spain. *Nat. Hazards Earth Syst. Sci.* 19, 1215–1234 (2019).
- Prodhan, F. A. et al. Projection of future drought and its impact on simulated crop yield over South Asia using ensemble machine learning approach. Sci. Total Environ. 807, 151029 (2022).
- Wang, A. et al. Global cropland exposure to extreme compound drought heatwave events under future climate change. Weather Clim. Extremes 40, 100559 (2023).
- Wang, B. et al. Probabilistic analysis of drought impact on wheat yield and climate change implications. Weather Clim. Extrem. 45, 100708 (2024).
- 23. Mondal, S. K. et al. Climate change will aggravate South Asian cropland exposure to drought by the middle of 21st century. *Earth's*. *Future* **12**, e2023EF003872 (2024).
- Schillerberg, T. A. & Tian, D. Global assessment of compound climate extremes and exposures of population, agriculture, and forest lands under two climate scenarios. *Earth's. Future* 12, e2024EF004845 (2024).
- Eyring, V. et al. Esmvaltool (v1.0) a community diagnostic and performance metrics tool for routine evaluation of earth system models in cmip. Geosci. Model Dev. 9, 1747–1802 (2016).
- Cherchi, A. et al. Global mean climate and main patterns of variability in the CMCC-CM2 coupled model. *J. Adv. Modeling Earth Syst.* 11, 185–209 (2019).
- 27. Rashid, H. A. et al. Evaluation of climate variability and change in ACCESS historical simulations for CMIP6. *J. South. Hemisph. Earth Syst. Sci.* **72**, 73–92 (2022).
- Pimonsree, S., Kamworapan, S., Gheewala, S., Thongbhakdi, A. & Prueksakorn, K. Evaluation of CMIP6 GCMs performance to simulate precipitation over Southeast Asia. *Atmos. Res.* 282, 106522 (2022).
- Luo, N., Guo, Y., Chou, J. & Gao, Z. Added value of CMIP6 models over CMIP5 models in simulating the climatological precipitation extremes in China. *Int. J. Climatol.* 42, 1148–1164 (2022).
- Song, S. & Yan, X. Evaluation of events of extreme temperature change between neighboring days in CMIP6 models over China. *Theor. Appl. Climatol.* 150, 53–72 (2022).
- Suthinkumar, P. S., Varikoden, H. & Babu, C. A. Assessment of extreme rainfall events over the Indian subcontinent during the historical and future projection periods based on CMIP6 simulations. *Int. J. Climatol.* 44, 39–58 (2024).

- Wang, T., Tu, X., Singh, V. P., Chen, X. & Lin, K. Global data assessment and analysis of drought characteristics based on CMIP6. *J. Hydrol.* 596, 126091 (2021).
- Wang, M. et al. Assessing urban flooding risk in response to climate change and urbanization based on shared socio-economic pathways. Sci. Total Environ. 880, 163470 (2023).
- Bjarke, N., Barsugli, J. & Livneh, B. CMIP6 derived ensemble of global vapor pressure defcit, potential evapotranspiration, and reference evapotranspiration. *Zenodo* https://doi.org/10.5281/ZENODO. 7789759 (2023).
- Bjarke, N., Barsugli, J. & Livneh, B. Ensemble of CMIP6 derived reference and potential evapotranspiration with radiative and advective components. Sci. Data 10, 417 (2023).
- Cao, B. et al. A 1 km global cropland dataset from 10 000 BCE to 2100 CE. Earth Syst. Sci. Data 13, 5403–5421 (2021).
- Chang, J., Li, Y., Wang, Y. & Yuan, M. Copula-based drought risk assessment combined with an integrated index in the Wei River Basin, China. J. Hydrol. 540, 824–834 (2016).
- Hao, Z. & Agha Kouchak, A. Multivariate standardized drought index: a parametric multi-index model. Adv. Water Resour. 57, 12–18 (2013).
- Hao, Z., Hao, F., Singh, V. P., Ouyang, W. & Cheng, H. An integrated package for drought monitoring, prediction and analysis to aid drought modeling and assessment. *Environ. Model. Softw.* 91, 199–209 (2017).
- Won, J., Choi, J., Lee, O. & Kim, S. Copula-based joint drought index using SPI and EDDI and its application to climate change. *Sci. Total Environ.* 744, 140701 (2020).
- 41. Fan, Y. R. et al. Characterizing the major contributors to the uncertainties in multi-hazard risks of compound extreme events. *Earth's. Future* **9**, e2021EF002280 (2021).
- Fan, Y. R., Yu, L. & Shi, X. Uncertainty quantification and partition for multivariate risk inferences through a Factorial Multimodel Bayesian Copula (FMBC) System. J. Hydrol. 598, 126406 (2021).

Acknowledgements

This research was supported by the National Natural Science Foundation of China (Grant No. 62073134).

Author contributions

Y.X. designed the research; X.W. collected all raw data; W.L. produced plots and tables; X.W., Y.X., and Y.F. conducted analysis; X.W. wrote the paper daft; all authors reviewed the manuscript.

Competing interests

The authors declare no competing interests.

Additional information

Supplementary information The online version contains supplementary material available at https://doi.org/10.1038/s44304-025-00144-w.

Correspondence and requests for materials should be addressed to Ye Xu.

Reprints and permissions information is available at http://www.nature.com/reprints

Publisher's note Springer Nature remains neutral with regard to jurisdictional claims in published maps and institutional affiliations.

Open Access This article is licensed under a Creative Commons Attribution-NonCommercial-NoDerivatives 4.0 International License, which permits any non-commercial use, sharing, distribution and reproduction in any medium or format, as long as you give appropriate credit to the original author(s) and the source, provide a link to the Creative Commons licence, and indicate if you modified the licensed material. You do not have permission under this licence to share adapted material derived from this article or parts of it. The images or other third party material in this article are included in the article's Creative Commons licence, unless indicated otherwise in a credit line to the material. If material is not included in the article's Creative Commons licence and your intended use is not permitted by statutory regulation or exceeds the permitted use, you will need to obtain permission directly from the copyright holder. To view a copy of this licence, visit http://creativecommons.org/licenses/by-nc-nd/4.0/.

© The Author(s) 2025